Supplement of Clim. Past, 21, 1895–1916, 2025
https://doi.org/10.5194/cp-21-1895-2025-supplement

Climate of the Past
Open Access
EGU

Supplement of

Global and regional sea-surface temperature changes over the Marine Isotopic Stage 9e and Termination IV

Nathan Stevenard et al.

Correspondence to: Nathan Stevenard (nathan.stevenard@univ-grenoble-alpes.fr)

Supplementary Information

S1. Spatio-temporal evolution of individual ΔSST records

In this section, we describe the spatio-temporal changes inferred from our new global-scale compilation of annual and seasonal SST anomalies relative to the PI period. **Figs. S1** and **S2** show each record time-binned every 1000 years based on the age-SST ensembles together with the uncertainty envelope representing the σ error (standard deviation) for each time bin. We refer to onset of the deglaciation as the beginning of the "strong" temperature rise visually defined. We also refer to interglacial "peak" all short periods (< 2 ka) displaying a distinct maximum temperature peak, while longer periods of maximum temperatures are refereed to "plateau". The term "glacial maximum" represents the lowest temperature within MIS 10.

S1.1 North Atlantic Basin

17 records from 10 sites are available to describe the temporal, spatial and timing of temperature changes in the North Atlantic basin over the T-IV and MIS 9 (**Fig. S1**). Most of the records are located in the eastern side of the basin, two sites are located in the central North Atlantic (DSDP-607 and U1313) and one in the North-western part (U1305).

The overall structure of SST temporal changes is similar over all the records as they are marked by a minimum SST value (i.e. glacial conditions) occurring during the period preceding T-IV, a fast increase over the deglacial period, an interglacial peak or plateau and finally a cooling phase, sometimes marked by a millennial-scale strong cooling at the end of the glacial inception. The only exception is the DSDP-607 SST record, which exhibits a continuous warming of summer and winter temperatures during the deglaciation. Intriguingly, this DSDP-607 site is located at the same site as the IODP site U1313, which shows annual temperatures (with a different proxy-based SST reconstruction) following the general pattern of variability as described above.

Glacial temperatures in the North Atlantic basin vary between -11 and -5°C relative to PI. The deglacial warming exhibits a range of 2.5 to 12°C (mean of ~7°C) to reach the interglacial peak or plateau. These interglacial conditions indicate, for most records, warmer temperatures compared to the PI, with a range between -2 to 4.5°C (mean of ~1.5°C).

The East and West subpolar North Atlantic (U1305, ODP-982, ODP-980) appear to warm earlier than the other sites and reach an interglacial peak between 338 and 340 ka. Other sites exhibit an interglacial peak at around 334-335 ka, with the exception of the DSDP-607 site which reaches the interglacial conditions at 331 ka.

The sites with multiple SST records indicate a similar range of variability (within the SST uncertainties). IODP site U1305 shows a consistent signal between the four records during the interglacial plateau, but also discrepancies before and after it. The case of core MD03-2699 shows the reverse scenario, with consistent values between the two records during the glacial maximum, but significant differences (~3.5°C) during the interglacial period.

S1.2 North Pacific basin

We isolate the North Pacific from the equatorial one, keeping 13 SST records (8 sites; **Fig. S1**) for this basin. Among these records, two are located in the eastern part of the basin (ODP-1012 and ODP-1020), one in the central North

(MD01-2416), while the others are located in the western part of the basin including three sites in the China Sea (ODP-1144, ODP-1146 and MD05-2901).

The temporal structure of the records is characterized by a glacial "maximum", clearly marked in the eastern part of the basin, but sometimes hidden by the prior variability (**Fig. S1**). Except for the $\delta^{18}O_p$-based SST record of core MD06-3074B, the deglacial warming is continuous. The $U_{37}^{K'}$ –based SST records from ODP sites 1020 and 1012, and IODP site U1429 exhibit two steps during the deglaciation: one characterized by slow and continuous warming, the other by an abrupt warming up to the interglacial conditions. The interglacial is rarely marked by a peak (ODP-1012, Mg/Ca from U1429) and is most often a plateau followed by a slow cooling. An exception is the $\delta^{18}O_p$-based SST record from MD06-3074B, which exhibits neither an interglacial plateau nor peak.

Glacial maximum temperatures cover a large range from -8 to 2°C relative to the PI (**Fig. S1**). The deglacial warming ranges from 2.5 to 7°C (mean of ~4.5°C) and reaches the interglacial peak or plateau. This latter period is characterized by highly heterogeneous temperatures ranging from -2 to 8°C (mean of 2°C) relative to the PI. After the optimum, sites ODP-1144, ODP-1146, U1429, ODP-1012, MD05-2901 and MD06-3074B (Mg/Ca-based SST record) exhibit temperatures throughout the glacial inception within the range estimated for the PI.

While we observe some heterogeneous SST amplitudes, the timing of the changes is relatively homogeneous (**Fig. S1**), with the exception of the $\delta^{18}O_p$-based SST record of core MD06-3074B. For the two sites located in the eastern part of the basin, deglaciation starts at around 341 ka. For the other sites, it starts at approximately ~338 ka. The interglacial conditions are attained between 331 and 334 ka, within the range of the chronological uncertainties.

For sites with multiple SST records, the variability often differs in terms of shape (e.g., MD06-3074B or ODP site 1146) or amplitude (e.g., IODP site U1429, ODP site 1146, MD06-3074B, and MD05-2901). IODP site U1429, with three SST proxies, shows a consistent SST signal among them, except for anomalously warmer conditions (up to 9 °C warmer than the PI) during the interglacial peak recorded in the Mg/Ca-based SST record. We note that the SST from $\delta^{18}O_p$-based SST records in the Northwest Pacific (primarily in the China Sea) show warmer conditions during the glacial period than the other sites or proxies.

S1.3 Equatorial Pacific

We define the Equatorial Pacific (between 10°N and 10°S) with 20 SST records (15 sites; Fig 3). The eastern Equatorial Pacific is represented with the ODP sites 677, 846, 1239, and cores TR163-19, RC13-110 and V19-30. Other sites are located west of the basin and one site (ODP-1143) is in the China Sea.

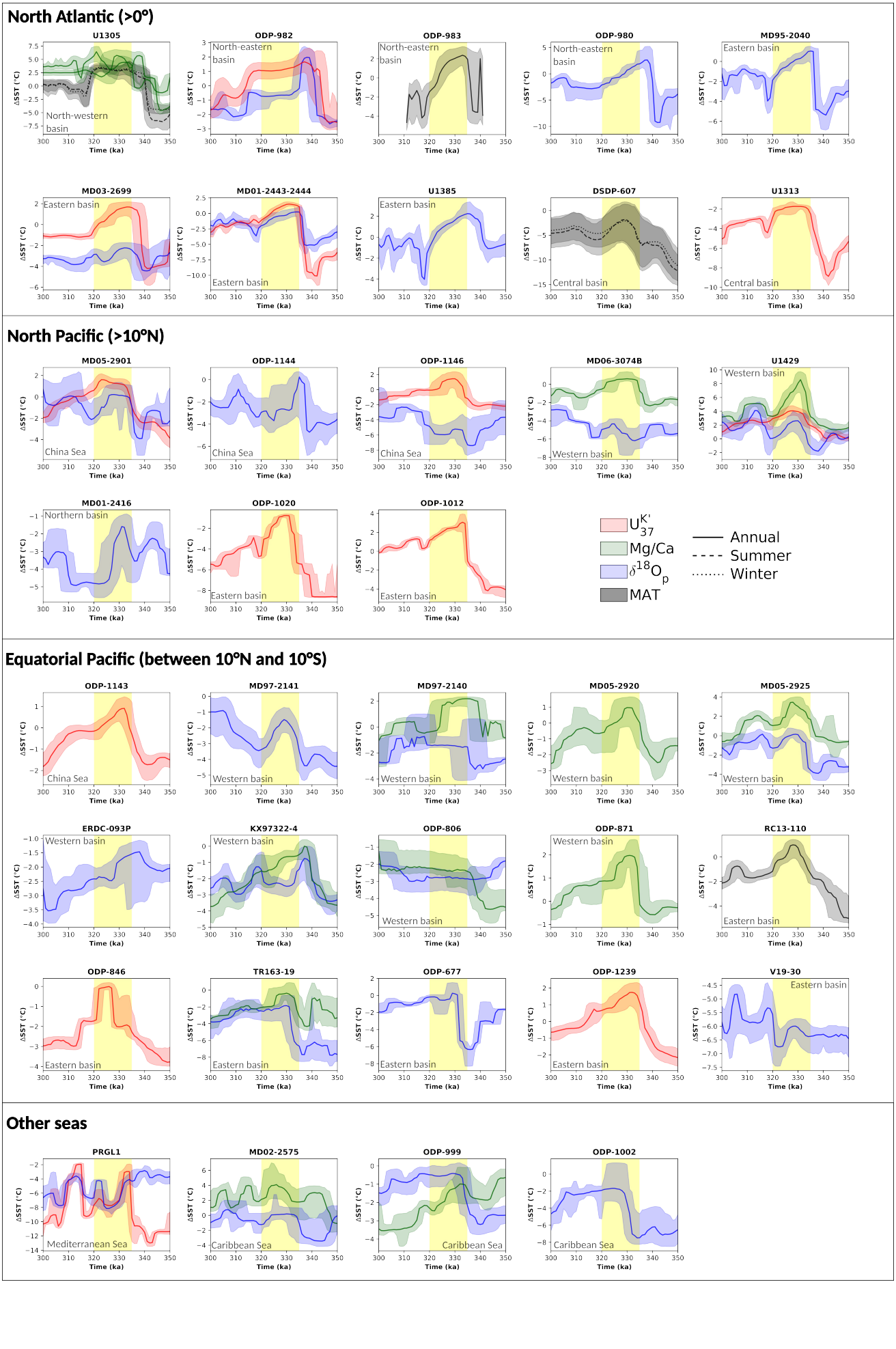
North Atlantic (>0°)
U1305
North-western basin
ODP-982
North-eastern basin
ODP-983
North-eastern basin
ODP-980
North-eastern basin
MD95-2040
Eastern basin
MD03-2699
Eastern basin
MD01-2443-2444
Eastern basin
U1385
Eastern basin
DSDP-607
Central basin
U1313
Central basin
North Pacific (>10°N)
MD05-2901
China Sea
ODP-1144
China Sea
ODP-1146
China Sea
MD06-3074B
Western basin
U1429
Western basin
MD01-2416
Northern basin
ODP-1020
Eastern basin
ODP-1012
Eastern basin
$U^{K'}_{37}$
Mg/Ca
$\delta^{18}O_p$
MAT
Annual
Summer
Winter
Equatorial Pacific (between 10°N and 10°S)
ODP-1143
China Sea
MD97-2141
Western basin
MD97-2140
Western basin
MD05-2920
Western basin
MD05-2925
Western basin
ERDC-093P
Western basin
KX97322-4
Western basin
ODP-806
Western basin
ODP-871
Western basin
RC13-110
Eastern basin
ODP-846
Eastern basin
TR163-19
Eastern basin
ODP-677
Eastern basin
ODP-1239
Eastern basin
V19-30
Eastern basin
Other seas
PRGL1
Mediterranean Sea
MD02-2575
Caribbean Sea
ODP-999
Caribbean Sea
ODP-1002
Caribbean Sea
ΔSST (°C)
Time (ka)

Figure S1: SST anomalies relative to PI for sites located in the North Atlantic, North Pacific, Equatorial Pacific and "Other seas". The SST proxies are the $U_{37}^{K'}$ (red), the Mg/Ca ratio (green), the $\delta^{18}O_p$ (blue), the MAT (black). These records are mixed between annual (solid lines), summer (dashed lines) and winter (dotted lines) SSTs. All records are time-binned every 500 years to take into account the age uncertainties. Yellow boxes represent the "optimum" interval as suggested by ice-core records. All records exhibit an envelop, that is the s uncertainty taking both age and SST uncertainties.

The six sites from the eastern basin exhibit similar temporal variability, with the exception of the ODP site 677 SST record which shows a strong cooling before the deglacial warming and core V19-30 where the MIS 9e peak is missing. Other eastern sites exhibit gradual warming, without a marked glacial maximum (or earlier than 350 ka). The end of the deglacial period is marked by a particularly fast warming in the record from ODP site 846. Once the interglacial plateau or peak is attained, the SST gradually cools during the glacial inception, except for the ODP site 846 where a strong cooling is visible after the optimum. On the other side (western) of the basin, the temporal variability is highly heterogeneous. In particular, a few $\delta^{18}O_p$-based SST records from sites off the New Guinea coast exhibit variability that deviates from the regional pattern in terms of variability. However, except for these records and the $\delta^{18}O_p$-based SST from core MD05-2925 which shows an abrupt warming, the other SST records exhibit a glacial "maximum" followed by a gradual deglacial warming. The optimum is partially a plateau (or pseudo-plateau) and partially a peak. This optimum is followed by a gradual cooling during the glacial inception, except for the ODP site 806, which tends to gradually warm.

The eastern sites show glacial temperatures ranging between -8 and -3°C at their minimum. The deglacial warming range varies between 3.5 and 7°C (mean of 5°C) for the eastern part of the Equatorial Pacific. The interglacial values are generally slightly colder than or equal to the PI period, except for the two sites RC13-110 and ODP-1239. For the western side of the basin, the temperature during the glacial maximum (if well defined) varies between -8 and 0°C (mean of -3°C) relative to the PI. The deglacial warming ranges between 1 and 6.5°C (mean of ~3.5°C). The SST during the interglacial peak or plateau is heterogeneous, with estimates varying from -3 to 3°C.

In the eastern basin, the deglacial warming starts at different dates, from ~ 348 ka (RC13-110 and ODP-846), ~ 343 ka (ODP-1239) or ~336 ka (TR163-19 and ODP-677). Despite this heterogeneity in deglacial warming, the climatic optimum is attained at around ~331 ka for all eastern sites, except for the ODP site 846 which exhibits a late interglacial plateau starting at ~328 ka. The duration of this optimum is, however, similar (about 3 to 4 ka) between these sites. In the western basin, SST records indicate a deglacial warming starting at around 341 ka, with a few exceptions ($\delta^{18}O_p$ from TR163-19 and ODP-871 records) which start at ~339 ka. The optimum is generally attained at around ~332 ka, but some sites (ERDC-093P, MD97-2140, MD05-2925 and KX97322-4 records) exhibit an earlier interglacial peak or plateau at around ~338 ka. The duration of the optimum conditions is generally about ~5 ka, but three sites (TR163-19, MD05-2925 and MD97-2140) show longer plateaus lasting between 7 and 11 ka.

The sites with multiple SST records from different proxies generally show colder SST estimates with $\delta^{18}O_p$-based reconstructions. This same tracer sometimes shows inconsistent temporal SST variability, as particularly observed in the ODP site 806 and MD97-2140 records, where no interglacial peak is recorded.

S1.4 Other sites

The "other sites" (**Fig. S1**) include sediment cores located in the Caribbean Sea (MD02-2575, ODP-999 and ODP-1002) and the Mediterranean Sea (PRGL1) that cannot be integrated into the regional basins described in this section.

In the Caribbean Sea, the temporal evolution of the $\delta^{18}O_p$-based SST records shows similar patterns, with a well-defined glacial maximum for ODP sites 999 and 1002, a slow deglacial warming and an interglacial plateau. However, Mg/Ca-based SST records exhibit different variability, with warmer or similar conditions during the glacial "maximum" compared to the interglacial. In the Mediterranean Sea, the deglacial warming is abrupt ($U^{K'}_{37}$-based SST record). The interglacial peak is directly followed by an abrupt cooling.

In the Caribbean Sea, the deglacial warming ranges from 1 to 5.5 °C (mean of 3°C). The interglacial conditions are similar to or colder than the PI (range from -2 to 4°C). In the Mediterranean Sea, the abrupt deglacial warming exhibits a 10°C difference between glacial and interglacial conditions. The interglacial, however, shows a -3°C anomaly relative to the PI.

The timing of the deglacial warming in the Caribbean Sea shows strong discrepancies, with a start between 340 and 349 ka. The date when interglacial conditions are attained is more constrained, at around ~332 ka (except for the Mg/Ca-based SST record from MD02-2575 where it is not well defined). In the Mediterranean Sea, the deglacial warming shown by the $U^{K'}_{37}$-based SST record starts at ~341 ka, with an abrupt SST increase at ~335 ka. The interglacial peak is attained immediately after this warming, at 334 ka, followed by a cooling at ~332 ka.

Three of the four sites have multiple SST records (**Fig. S1**). The PRGL-1 records indicate consistent variability and values between them, with the exception of the "cold" periods (i.e. Glacial maximum and the end of the glacial inception) where the $\delta^{18}O_p$-based SST record exhibits anomalously warmer temperature. The two sites (MD02-2575 and ODP-999) in the Caribbean Sea show strong discrepancies between their two respective records in terms of temporal variability, anomaly values and timing of changes, making it difficult to reconcile these records.

S1.5 South Atlantic

16 SST records are located in the South Atlantic region (13 sites; **Fig. S2**) in this synthesis. These sites are concentrated in particular in the South-eastern part of the basin, close to the junction between the Indian and the Atlantic Oceans.

For most of the sites, the glacial maximum conditions are dated earlier than the studied period (> 350 ka) and only the SST record of core MD02-2588 shows a distinct glacial maximum. The SST records at sites GeoB1113-4, PS2489-2 ODP-1089, MD96-2085, RC12-294 and TN057-06 exhibit a continuous deglacial warming. Other sites show abrupt warming during the deglaciation. The optimum is marked by a peak in most of the sites, but a plateau is observed in the MD96-2094, ODP-1084, RC12-294, ODP-1089 and MD96-2085 records. This period is followed by a slow and continuous cooling, with a few exceptions of an abrupt cooling at the end of the optimum (ODP-1089, ODP-1090, TN057-06, GeoB1113-4 and MD96-2094).

As only one glacial maximum is observed, it is difficult to define a range of SST values. However, the MD02-2588 record shows temperatures -3°C colder than those of the PI. The deglacial warming amplitude ranges between 2 and 9°C (mean of ~3.5). The interglacial peak (or plateau) values range from -1.5 to 4°C (mean of ~1°C) relative to the PI. The sites that show abrupt cooling after the optimum exhibit a 2 to 4°C cooling during the glacial inception.

Due to the missing glacial maximum in most records, the timing of the start of the deglacial warming appears to be older than 350 ka. The interglacial conditions are attained between 333 and 336 ka for a few sites (MD02-2588, RC12-294, ODP-1084 and GeoB1113-4). The other sites show an earlier interglacial, mostly attained between 338 and 340

ka. The duration of the interglacial plateau is heterogeneous, ranging between ~4 ka (ODP-1090) and ~21 ka (ODP-1084), but most often around ~6 ka.

Sites with multiple SST proxies (MD96-2080 and ODP-1089) indicate inconsistent temporal variability and SST values between them. Site MD96-2080 shows similar optimum values between Mg/Ca-based and $\delta^{18}O_p$-based SST, but they are asynchronous. MAT data from site ODP-1089 does not show any warming before the interglacial peak (not covered in this record) and indicates warmer conditions compared to $\delta^{18}O_p$-based SST.

S1.6 South Pacific

Nine SST records are located in the South Pacific (>10°S, 7 sites; **Fig. S2**). Sites GeoB3327-5 and PS75-034-2 are located in the eastern part of the basin, while the others are located off the coasts of New Zealand or Tasmania.

Except for the ODP-1172 and MD06-2986 sites, all SST records show a similar temporal variability. These variations are characterized by a well-defined glacial climate, followed by an abrupt deglacial warming. Site MD97-2120 ($\delta^{18}O_p$-based SST), however, exhibit a slightly less abrupt warming. The climate optimum appears as a short peak in most of SST records. Only the PS75-034-2 site shows an interglacial plateau. The glacial inception is characterized by a continuous cooling, except for a few sites (PS75-034-2 and Mg/Ca-based SST records from ODP-1172 and MD97-2120) which exhibit an abrupt cooling.

The glacial SST values are strongly heterogeneous, ranging from -7 (ODP-1172) to 0°C (ODP-1123) relative to the PI. The amplitude of the deglacial warming varies between 3 and 6.5°C (mean of ~5°C). The interglacial period is characterized by temperatures warmer than the PI, except for records from ODP site 1172, which indicate a -3°C (excluding $\delta^{18}O_p$-based SST record) anomaly relative to the PI. Hence, these interglacial values vary from -3 to 6°C relative to the PI.

The deglacial warming generally starts between 340 and 345 ka, with an exception at site ODP-1172 (336 ka). The interglacial maximum SST anomaly values are synchronized between the sites and are attained between 333 and 336 ka. Site PS75-034-2, the only one showing an interglacial plateau, exhibits “warm” conditions lasting for ~8 ka.

The two sites (MD97-2120 and ODP-1172) with multiple SST records show either good agreement (MD97-2120), or completely different variability and range of SST anomalies (ODP-1172). Intriguingly, the $\delta^{18}O_p$-based SST record from ODP site 1172 exhibits its coldest value during the interglacial peak, while the glacial inception shows a continuous warming. This signal strongly differs from the Mg/Ca record from the same site.

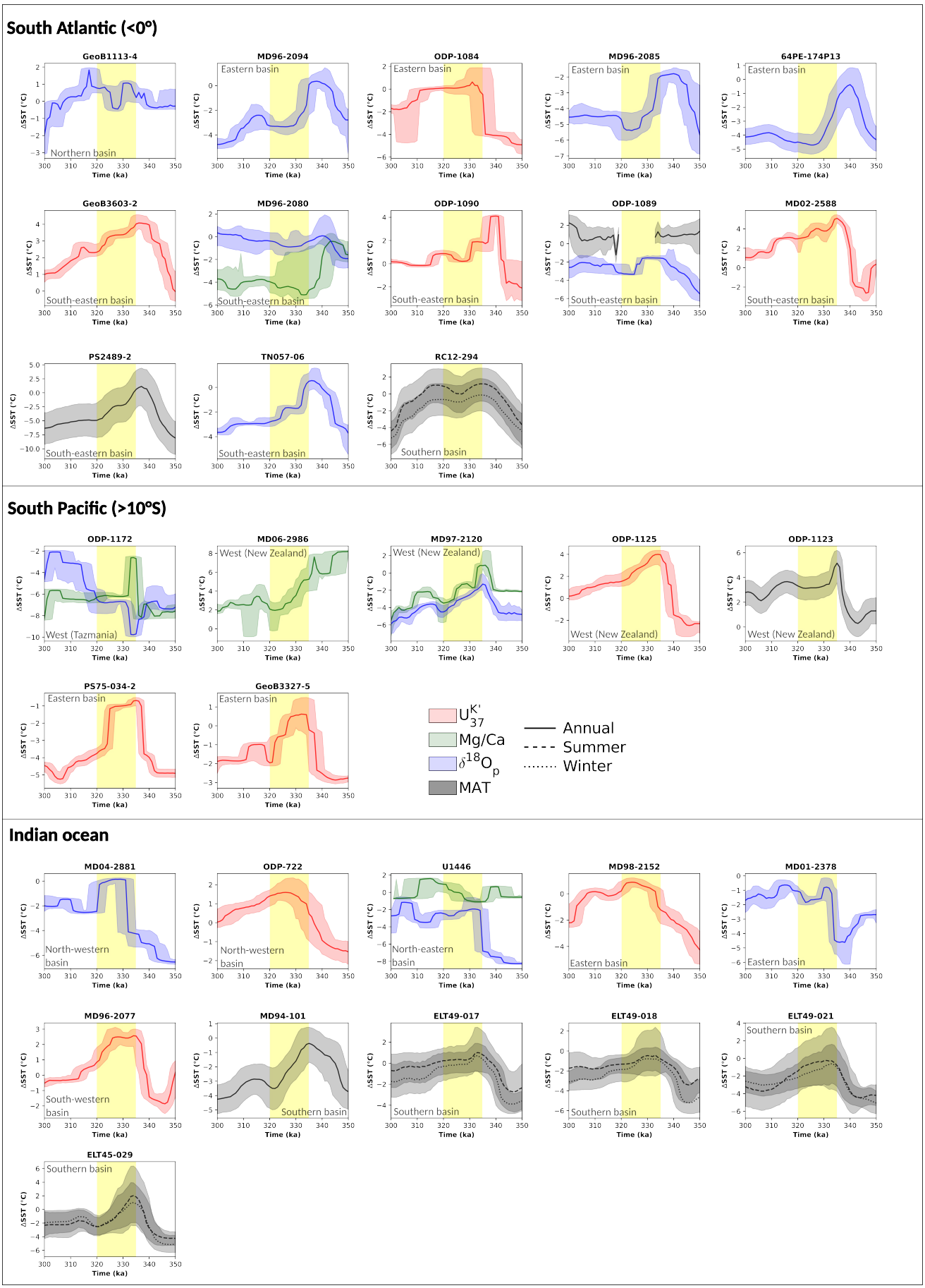

Figure S2: same as Fig. S1 but for the South Atlantic, South Pacific and Indian basins.

S1.7 Indian Ocean

16 SST records are available in the Indian Ocean (11 sites; **Fig. S2**). One site (MD96-2077) is located in the southwestern side of the basin, two (MD98-2152 and MD01-2378) in the eastern side, five (ELT cores and MD94-101) in the south, and three (MD04-2881, U1446 and ODP-722) in the north.

We observe two different types of temporal structure amongst those SST records. The first type is characterized by a slow and continuous deglacial warming (the four ELT cores, MD94-101, MD98-2152 and ODP-722). The other type is characterized by an abrupt deglacial warming (MD04-2881, U1446, MD96-2077 and MD01-2378), sometimes preceded by a slow and continuous warming (MD04-2881 and $\delta^{18}O_p$-based SST record from U1446). The interglacial optimum is rarely a peak (ELT45-029, MD94-101 and MD01-2378) and is more often represented as a plateau, sometimes marked by a slight cooling. The glacial inception is characterized by a slow cooling, except for sites MD04-2881 and MD94-101 which exhibit a strong cooling at the end of the peak or plateau.

The coldest conditions before the interglacial peak or plateau are generally about -4°C (range from -5 to -1.5°C) relative to the PI. The deglacial warming ranges between 2.5 and 7°C (mean of ~4°C). The Indian Ocean appears to be warmer than 1°C compared to the PI, with all SST anomaly values equal to or greater than 0°C.

In most records, the deglacial warming starts at around ~346 ka or before 350 ka (MD94-101, MD98-2152, ELT45-029 and ODP-722). Only one record (MD01-2378) indicates a late warming at ~336 ka. The interglacial peak or plateau is attained between 330 and 334 ka, except for site the record from MD96-2077 (~336 ka). For sites exhibiting an interglacial plateau, the duration of these conditions varies between 8 and 11 ka.

Only one site (U1446) has multiple annual SST records in this basin. The $\delta^{18}O_p$-based SST record shows consistent temporal patterns, values and timing of temperature variations. However, the Mg/Ca-based SST record exhibits a very different variability, with warmer conditions during the deglacial warming than the SST derived from $\delta^{18}O_p$. Despite these differences, the glacial inception agrees in term of range of temperature between the two records, but the structures are quite different.

S1.8 Selection of records

We have chosen to exclude a few records from the stacking process (see section 3.1 in the main text). The selection of these records is based on the description above. We exclude records which present: 1) a very different pattern of variability from the regional trend and 2) a too different SST estimates compared to SST based on another proxy from the same site. This include nine $\delta^{18}O_p$-based SST records (ODP-1146, MD06-3074B, MD03-2699, MD01-2416, ODP-806, MD02-2575, ODP-1172 and V19-30) and four Mg/Ca-based SST records (ODP-999, MD96-2080, MD06-2080 and U1446).

S2. Chronologies

This section gives supplementary information (**Figs. S3-5**). **Fig. S3** shows the comparison between GL_T_syn (Barker et al., 2011) and CH_4 record (Loulergue et al., 2008; Nehrbass-Ahles et al., 2020). Fig S4 exhibits the alignment of each site (blue curve) to its reference (black curve). **Fig S5** displays the final age model with uncertainties.

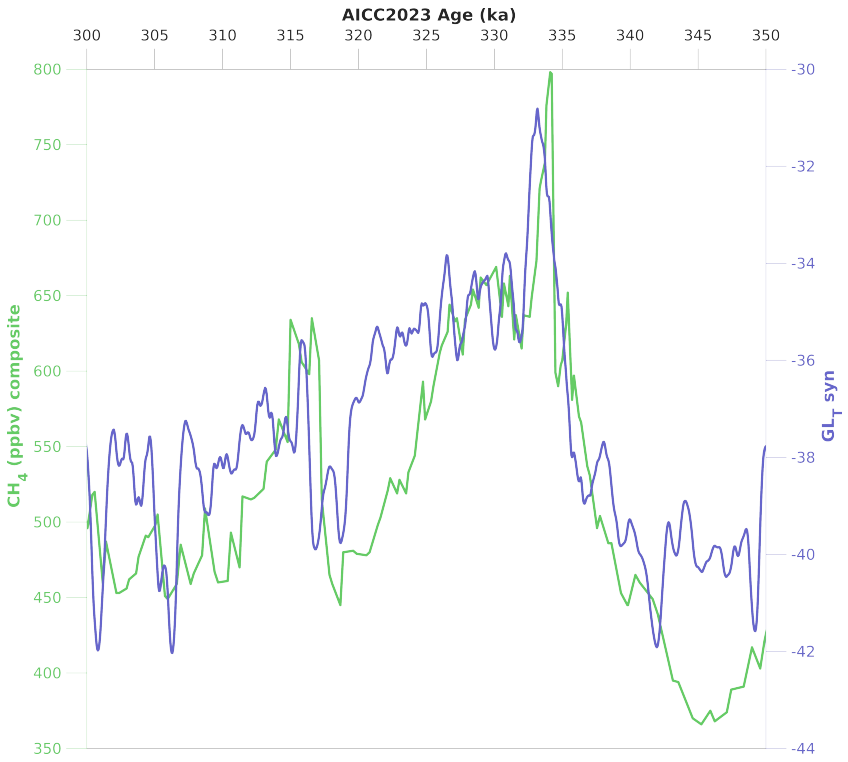

Figure S3: Comparison between the atmospheric CH_4 concentration (Loulergue et al., 2008; Nehrbass-Ahles et al., 2020) and synthetic curve of Greenland temperatures GL_T_syn (Barker et al., 2011). The two records are displayed on the AICC2023 chronology (Bouchet et al., 2023)

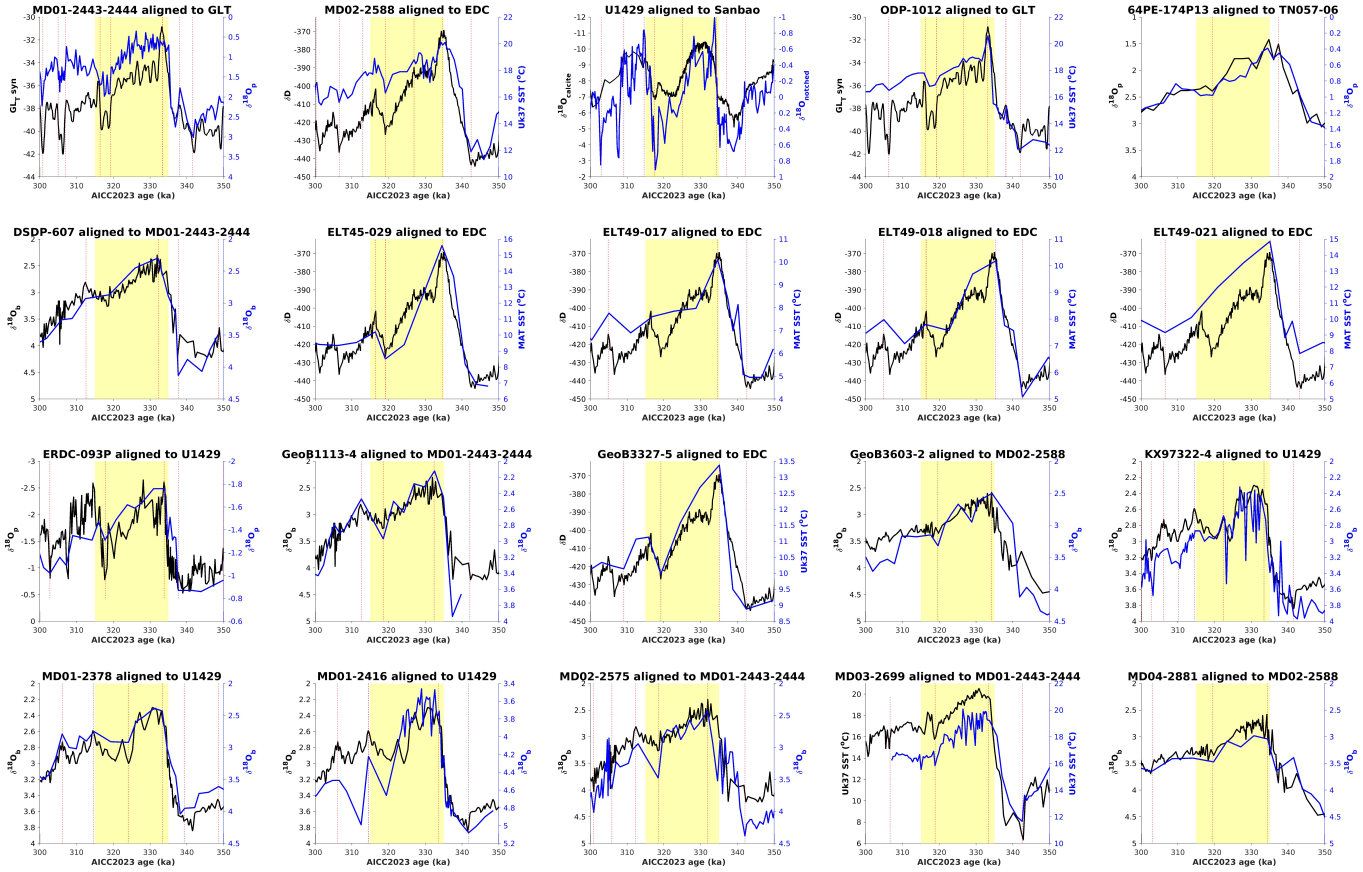

Figure S4: Alignments of the SST sites used in this study. For each plot, the blue line represents the record used to align to the reference (black line). The dotted vertical lines are the tie-points as defined in the *AnalySeries* software (Paillard et al., 1996). The light yellow area in each plot envelops the MIS 9e.

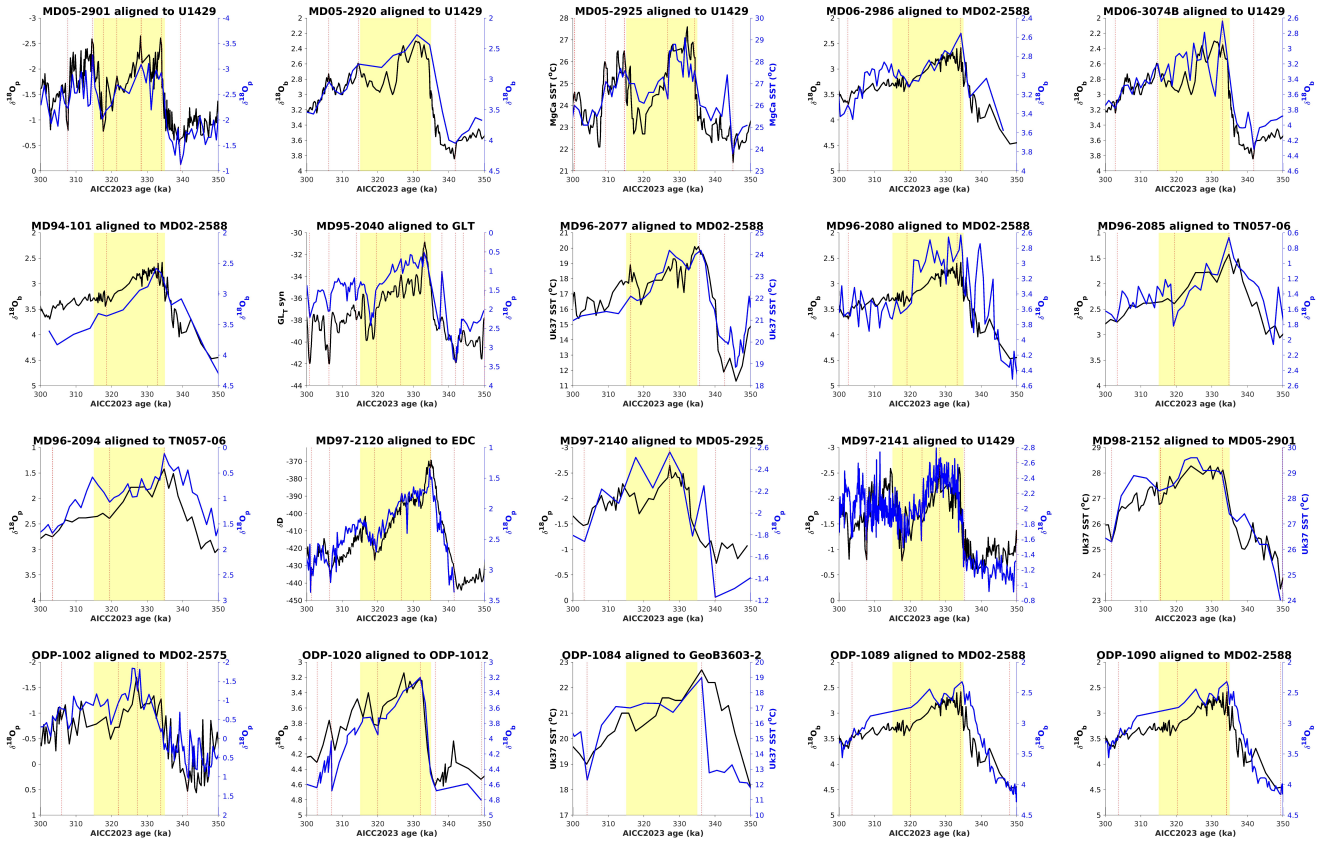

Figure S4 (suite)

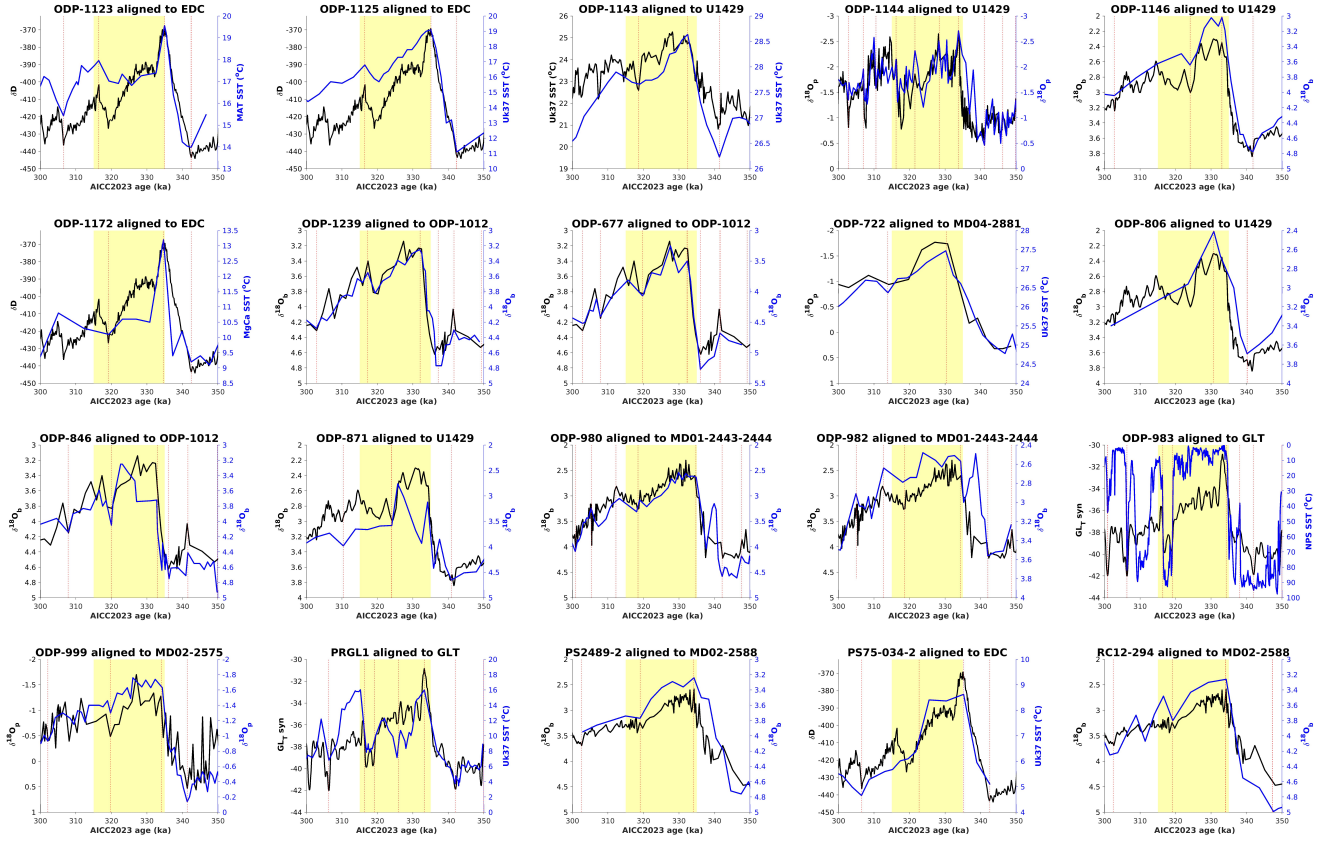

Figure S4 (suite)

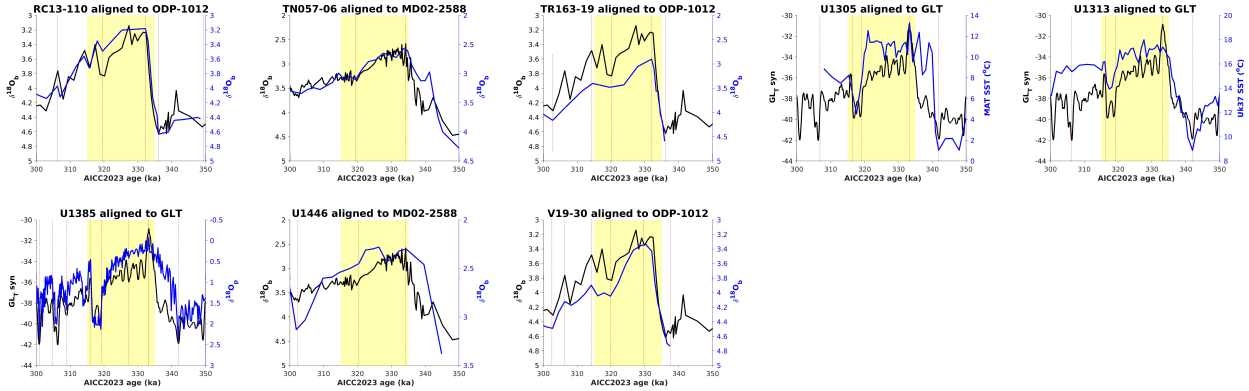

Figure S4 (suite)

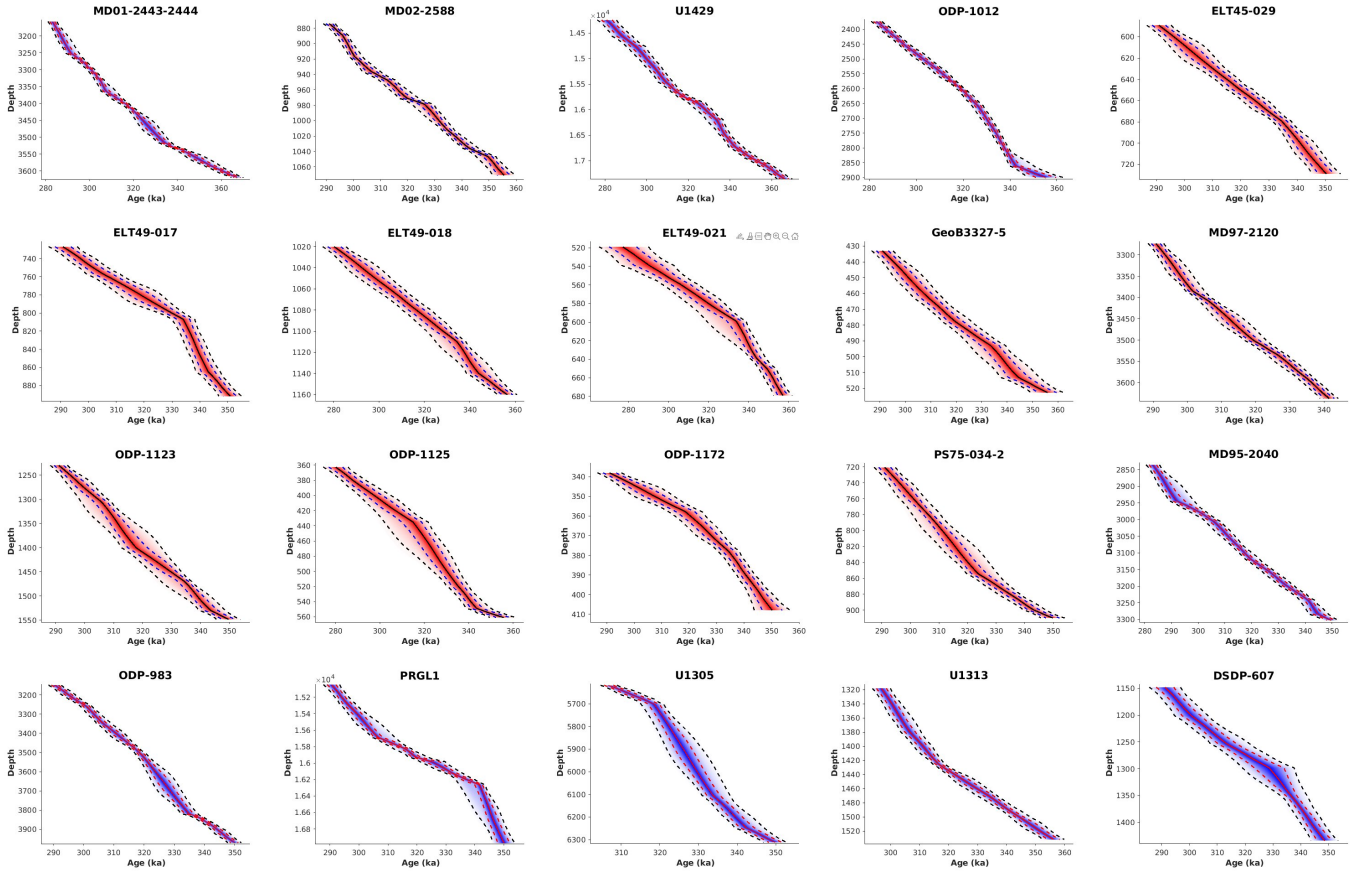

Figure S5: Results of the final Bayesian age-depth models using the "Undatable" GUI software (Lougheed and Obrochta, 2019). The middle line represents the median age. The dotted lines represent the σ and 2σ uncertainties. The color is defined under latitudinal criteria: The northern sites (latitude > 23.5) are plotted in blue, the tropical sites (latitude between 23.5 and -23.5) are plotted in green and the southern sites (latitude < -23.5 are plotted in red).

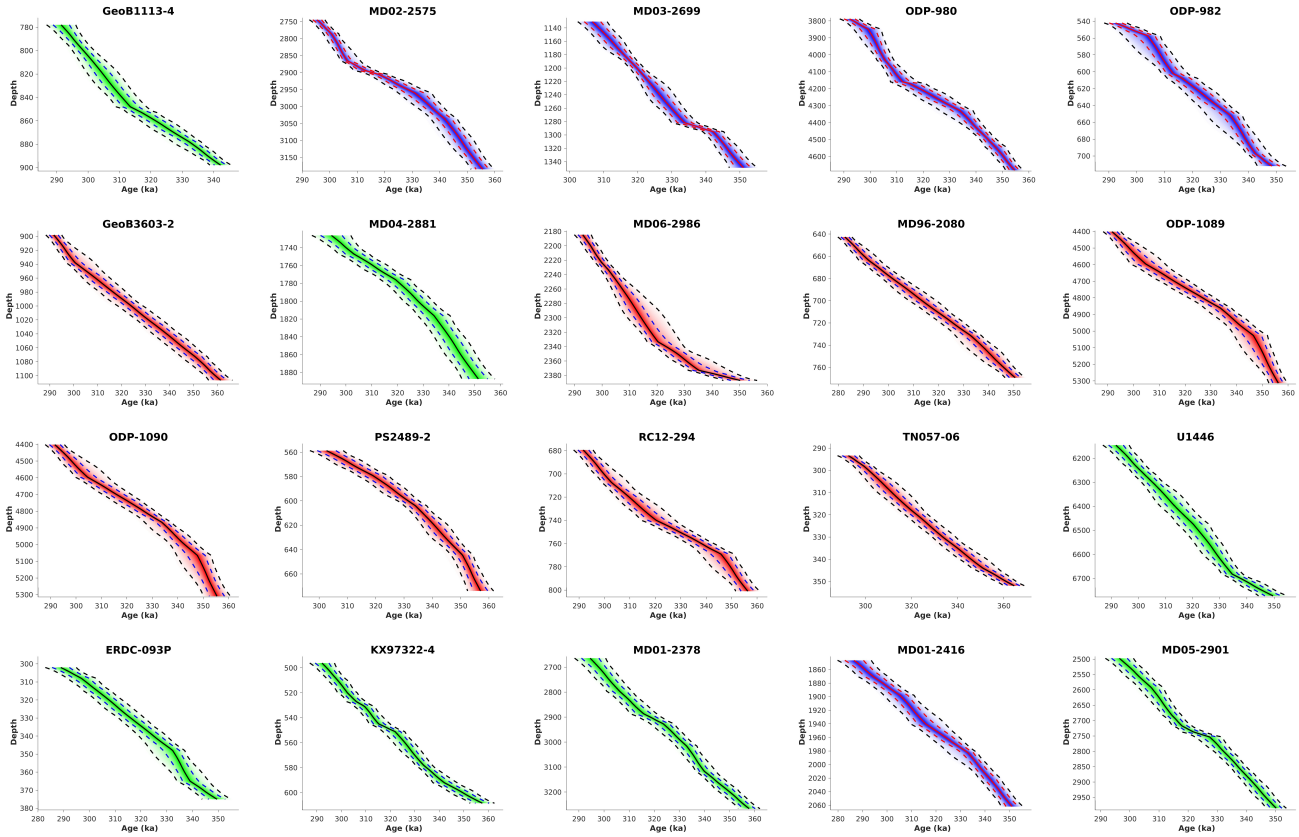

Figure S5 (suite)

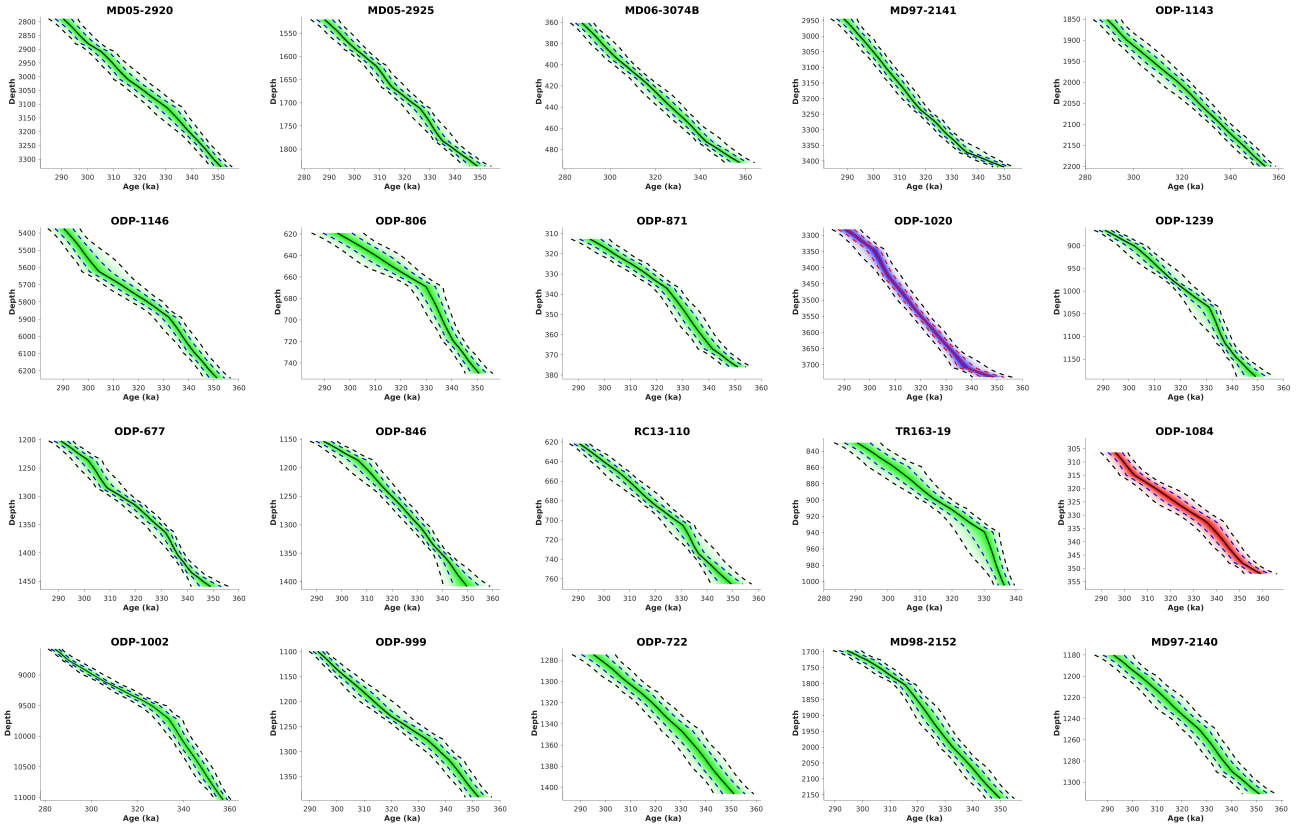

Figure S5 (suite)

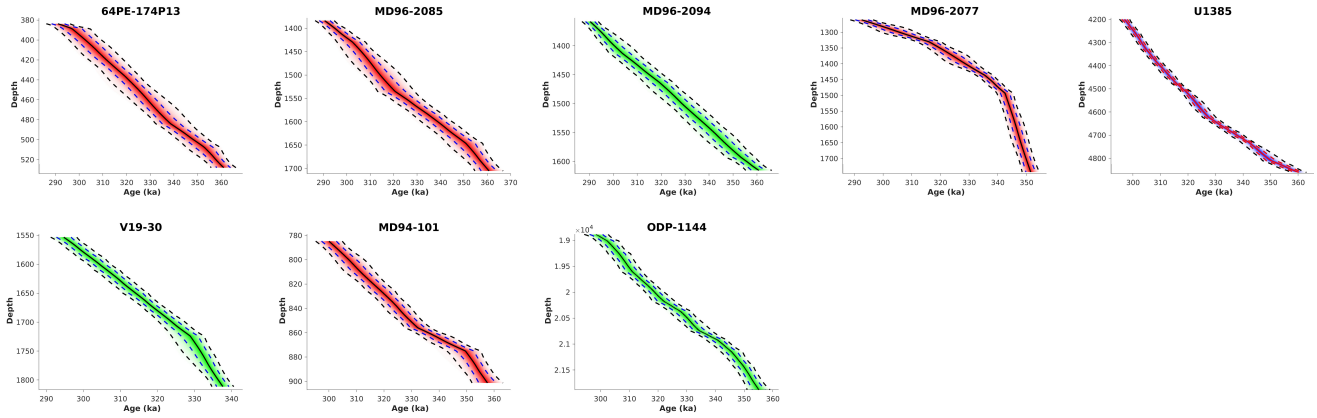

Figure S5 (suite)

S3. Site information

Table S1 : Locations, available proxies used in this study, SST type and original references of the sites used in this study. The lines with bold text indicate the four "basin references".

Core_name	Basin	Latitude	Longitude	Elevation (m)	Proxy	Species	SST type	Published ution (ka)	Reference
64PE-174P13	South Atlantic	-29,76	2,40	-2912	$\delta^{18}O$	*G. ruber*	Seasonnal	1,87	[1]
DSDP-607	North Atlantic	41,00	-32,96	-3427	MAT	*Na*	Seasonnal	2,82	[2]
ELT45-029	Indian	-44,88	106,52	-3867	MAT	*Na*	Seasonnal	3,50	[3]
ELT49-017	Indian	-48,28	90,25	-3546	MAT	*Na*	Seasonnal	3,85	[3]
ELT49-018	Indian	-46,05	90,16	-3282	MAT	*Na*	Seasonnal	2,31	[3]
ELT49-021	Indian	-42,19	94,89	-3319	MAT	*Na*	Seasonnal	3,97	[3]
ERDC-093P	Equatorial Pacific	-2,24	157,01	-1604	$\delta^{18}O$	*T. sacculifer*	Annual	2,24	[4]
GeoB1113-4	South Atlantic	-5,75	-11,04	-2374	$\delta^{18}O$	*G. ruber*	Annual	2,15	[5]
GeoB3327-5	South Pacific	-43,24	-79,99	-3531	$U^{K'}_{37}$	*Na*	Annual	3,66	[6]
GeoB3603-2	South Atlantic	-35,13	17,54	-2840	$U^{K'}_{37}$	*Na*	Annual	1,55	[7]
KX97322-4	Equatorial Pacific	-0,03	159,25	-2362	$\delta^{18}O$	*G. ruber*	Annual	0,52	[8]
KX97322-4	Equatorial Pacific	-0,03	159,25	-2362	Mg/Ca	*G. ruber*	Annual	0,52	[8]
MD01-2378	Indian	-13,08	121,79	-1783	$\delta^{18}O$	*G. ruber*	Annual	2,32	[9]
MD01-2416	North Pacific	51,27	167,73	-2317	$\delta^{18}O$	*N. pachyderma*	Annual		[10]
MD01-2443-	North Atlantic	**37,69**	**-10,15**	**-2790**	**$U^{K'}_{37}$**	*Na*	**Annual**	**0,39**	[11]
MD01-2443-	North Atlantic	**37,69**	**-10,15**	**-2790**	**$\delta^{18}O$**	*G. bulloides*	**Annual**	**0,38**	[12]
MD02-2575	Caribbean	29,00	-87,12	-847	Mg/Ca	*G. ruber*	Annual	0,77	[13]
MD02-2575	Caribbean	29,00	-87,12	-847	$\delta^{18}O$	*G. ruber*	Annual	0,77	[13]
MD02-2588*	South Atlantic	**-41,20**	**25,50**	**-2907**	**$U^{K'}_{37}$**	*Na*	**Annual**	**0,47**	[14]
MD03-2699	North Atlantic	39,04	-10,66	-1865	$U^{K'}_{37}$	*Na*	Annual	0,65	[15]
MD03-2699	North Atlantic	39,04	-10,66	-1865	$\delta^{18}O$	*G. inflata*	Annual	0,53	[16]
MD04-2881	Indian	22,20	63,08	-2387	$\delta^{18}O$	*G. ruber*	Annual	2,73	[17]
MD05-2901	North Pacific	14,38	110,74	-1454	$U^{K'}_{37}$	*Na*	Annual	0,96	[18]
MD05-2901	North Pacific	14,38	110,74	-1454	$\delta^{18}O$	*G. ruber*	Annual	0,96	[18]
MD05-2920	Equatorial Pacific	-2,86	144,53	-1849	Mg/Ca	*G. ruber*	Annual	0,83	[19]
MD05-2925	Equatorial	-9,34	151,46	-1661	Mg/Ca	*G. ruber*	Annual	1,09	[20]

MD05-2925	Pacific Equatorial Pacific	-9,34	151,46	-1661	$\delta^{18}O$	*G. ruber*	Annual	1,17	[20]
MD06-2986	South Pacific	-43,45	167,90	-1477	Mg/Ca	*G. bulloides*	Annual	1,14	[21]
MD06-3074B	North Pacific	17,01	124,81	-2510	Mg/Ca	*G. ruber*	Annual	2,77	[22]
MD06-3074B	North Pacific	17,01	124,81	-2510	$\delta^{18}O$	*G. ruber*	Annual	2,67	[22]
MD94-101	Indian	-42,50	79,42	-2920	MAT	*Na*	Seasonnal	1,92	*unpublished*
MD95-2040	North Atlantic	40,58	-9,86	-2465	$\delta^{18}O$	*G. bulloides*	Annual	0,47	[23]
MD96-2077	Indian	-33,28	31,42	-3781	$U^{K'}_{37}$	*Na*	Annual	2,33	[24]
MD96-2080	South Atlantic	-36,27	19,48	-2488	Mg/Ca	*G. bulloides*	Annual	1,24	[25]
MD96-2080	South Atlantic	-36,27	19,48	-2488	$\delta^{18}O$	*G. bulloides*	Annual	0,52	[25]
MD96-2085	South Atlantic	-29,70	12,94	-3001	$\delta^{18}O$	*G. inflata*	Annual	1,13	[26]
MD96-2094	South Atlantic	-20,00	9,27	-2280	$\delta^{18}O$	*G. inflata*	Annual		[27]
MD97-2120	South Pacific	-45,53	174,93	-1210	Mg/Ca	*G. bulloides*	Annual	1,44	[28]
MD97-2120	South Pacific	-45,53	174,93	-1210	$\delta^{18}O$	*G. bulloides*	Annual	0,36	[28]
MD97-2140	Equatorial Pacific	2,03	141,77	-2547	Mg/Ca	*G. ruber*	Annual	3,89	[29]
MD97-2140	Equatorial Pacific	2,03	141,77	-2547	$\delta^{18}O$	*G. ruber*	Annual	3,75	[29]
MD97-2141	North Pacific	8,78	121,28	-3633	$\delta^{18}O$	*G. ruber*	Annual	0,17	[30]
MD98-2152	Indian	-6,33	103,88	-1796	$U^{K'}_{37}$	*Na*	Annual	2,64	[31]
ODP-1002	Caribbean	10,71	-65,17	-893	$\delta^{18}O$	*G. ruber*	Annual	0,97	[32]
ODP-1012*	North Pacific	**32,28**	**-118,38**	**-1783**	**$U^{K'}_{37}$**	*Na*	**Annual**	**1,26**	[33]
ODP-1020	North Pacific	41,00	-126,43	-3042	$U^{K'}_{37}$	*Na*	Annual	2,38	[33]
ODP-1084	South Atlantic	-25,51	13,03	-1992	$U^{K'}_{37}$	*Na*	Annual	2,19	[34]
ODP-1089	South Atlantic	-40,94	9,89	-4621	$\delta^{18}O$	*G. bulloides*	Annual	0,48	[35]
ODP-1089	South Atlantic	-40,94	9,89	-4621	MAT	*Na*	Seasonnal	3,29	[36]
ODP-1090	South Atlantic	-42,91	8,90	-3702	$U^{K'}_{37}$	*Na*	Annual	2,99	[37]
ODP-1123	South Pacific	-41,79	-171,50	-3290	MAT	*Na*	Annual	1,89	[38]
ODP-1125	South Pacific	-42,55	-178,17	-1365	$U^{K'}_{37}$	*Na*	Annual	3,65	[39]
ODP-1143	North Pacific	9,36	113,29	-2772	$U^{K'}_{37}$	*Na*	Annual	1,32	[40]
ODP-1144	North Pacific	20,05	117,42	-2037	$\delta^{18}O$	*G. ruber*	Annual	0,63	[64]
ODP-1146	North Pacific	19,46	116,27	-2092	$U^{K'}37$	*Na*	Annual	1,65	[41]
ODP-1146	North Pacific	19,46	116,27	-2092	$\delta^{18}O$	*G. ruber*	Annual	1,63	[42]
ODP-1172	South Pacific	-43,96	149,93	-2622	Mg/Ca	*G. bulloides*	Annual	2,45	[43]
ODP-1172	South Pacific	-43,96	149,93	-2622	$\delta^{18}O$	*G. bulloides*	Annual	2,45	[43]
ODP-1239	Equatorial Pacific	-0,67	-82,08	-1414	$U^{K'}_{37}$	*Na*	Annual	1,16	[44]
ODP-677	Equatorial Pacific	1,20	-83,73	-3450	$\delta^{18}O$	*G. ruber*	Annual	2,5	[45]
ODP-722	Indian	16,62	59,80	-2034	$U^{K'}_{37}$	*Na*	Annual	1,06	[41]
ODP-806	Equatorial Pacific	0,32	159,36	-2520	Mg/Ca	*G. ruber*	Annual	3,82	[46]
ODP-806	Equatorial Pacific	0,32	159,36	-2520	$\delta^{18}O$	*G. ruber*	Annual	3,82	[46]
ODP-846	Equatorial Pacific	-3,10	-90,82	-3296	$U^{K'}_{37}$	*Na*	Annual	2,19	[41]
ODP-871	Equatorial Pacific	5,55	172,35	-1255	Mg/Ca	*G. ruber*	Annual	2,85	[47]
ODP-980	North Atlantic	55,48	-14,70	-2180	$\delta^{18}O$	*N. incompta*	Annual	0,83	[48]
ODP-982	North Atlantic	57,50	-15,87	-1135	$\delta^{18}O$	*G. bulloides*	Annual	2,31	[49]
ODP-982	North Atlantic	57,50	-15,87	-1135	$U^{K'}_{37}$	*Na*	Seasonnal	1,56	[50]
ODP-983	North Atlantic	60,40	-23,64	-1984	MAT	*Na*	Annual	0,78	[51]
ODP-999	Caribbean	12,75	-78,73	-2827	Mg/Ca	*G. ruber*	Annual	1,35	[52]
ODP-999	Caribbean	12,75	-78,73	-2827	$\delta^{18}O$	*G. ruber*	Annual	1,27	[52]

PRGL1	Mediterannean Sea	42,69	3,84	-299	$\delta^{18}O$	*G. bulloides*	Annual	0,61	[53]
PRGL1	Mediterannean Sea	42,69	3,84	-299	$U^{K'}_{37}$	*Na*	Seasonnal	0,46	[54]
PS2489-2	South Atlantic	-42,87	8,97	-3794	MAT	*Na*	Seasonnal	1,13	[55]
PS75-034-2	South Pacific	-54,37	-80,09	-4436	$U^{K'}_{37}$	*Na*	Annual	3,38	[6]
RC12-294	South Atlantic	-37,27	-10,10	-3308	MAT	*Na*	Seasonnal	2	[56]
RC13-110	Equatorial Pacific	-0,10	-95,65	-3231	MAT	*Na*	Annual	3,55	[57]
TN057-06	South Atlantic	-42,90	8,90	-3751	$\delta^{18}O$	*G. bulloides*	Annual		[58]
TR163-19	Equatorial Pacific	2,26	-90,95	-2348	Mg/Ca	*G. ruber*	Annual	1,65	[59]
TR163-19	Equatorial Pacific	2,26	-90,95	-2348	$\delta^{18}O$	*G. ruber*	Annual	1,57	[59]
U1305	North Atlantic	57,48	-48,53	-3460	Mg/Ca	*N. pachyderma*	Seasonnal	1,87	[60]
U1305	North Atlantic	57,48	-48,53	-3460	Mg/Ca	*N.incompta*	Seasonnal	1,87	[60]
U1305	North Atlantic	57,48	-48,53	-3460	MAT	*Na*	Seasonnal	0,91	[60]
U1313	North Atlantic	41,00	-32,96	-3426	$U^{K'}_{37}$	*Na*	Annual	0,56	[61]
U1385	North Atlantic	37,57	-10,13	-2587	$\delta^{18}O$	*G. bulloides*	Annual	0,18	[65]
U1429*	North Pacific	**31,62**	**129,00**	**-732**	**Mg/Ca**	*G. ruber*	**Annual**	**0,3**	[62]
U1429*	North Pacific	**31,62**	**129,00**	**-732**	**$U^{K'}_{37}$**	*Na*	**Annual**	**0,3**	[62]
U1429*	North Pacific	**31,62**	**129,00**	**-732**	**$\delta^{18}O$**	*G. ruber*	**Annual**	**0,3**	[62]
U1446	Indian	19,08	85,74	-1430	Mg/Ca	*G. ruber*	Annual	3,16	[63]
U1446	Indian	19,08	85,74	-1430	$\delta^{18}O$	*G. ruber*	Annual	2,13	[63]
V19-30	Equatorial Pacific	-3,38	-83,52	-3091	$\delta^{18}O$	*N. dutertrei*	Annual	0,33	[66]

[1] Scussolini & Peeters (2013); [2] Ruddiman et al. (1989); [3] Howard & Prell (1992); [4] Shackleton (1992); [5] Sarnthein et al. (1994); [6] Ho et al. (2012); [7] Peeters et al. (2004); [8] Zhang et al. (2021); [9] Holbourn et al. (2005); [10] Gebhardt et al. 2008; [11] Martrat et al. (2007); [12] Hodell et al. (2013); [13] Nürnberg et al. (2008); [14] Romero et al. (2015); [15] Rodrigues et al. (2011); [16] Voelker et al. (2010); [17] Ziegler et al. (2010); [18] Li et al. (2009); [19] Tachikawa et al. (2014); [20] Lo et al. (2017); [21] Mashiotta et al. (1999); [22] Jia et al. (2018); [23] Voelker & Abreu (2011); [24] Bard & Rickaby (2009); [25] Martínez-Méndez et al. (2010); [26] Chen et al. (2002); [27] Stuut et al. (2002); [28] Pahnke et al. (2003); [29] Garidel-Thoron et al. (2005); [30] Oppo et al. (2003); [31] Windler et al. (2019); [32] Gibson & Peterson (2014); [33] Hebert et al. (2001); [34] Rosell-Melé et al. (2014); [35] Hodell et al. (2003); [36] Cortese et al. (2004); [37] Martínez-Garcia et al. (2009); [38] Hayward et al. (2008); [39] Peterson et al. (2020); [40] Li et al. (2011); [41] Herbert et al. (2010); [42] Clemens et al. (2008); [43] Nürnberg & Groeneveld (2006); [44] Dyez et al. (2016); [45] Shackleton et al. (2011); [46] Medina-Elizalde & Lea (2005); [47] Dyez & Ravelo (2014); [48] McManus et al. (1999); [49] Venz et al. (1999); [50] Herbert et al. (2016); [51] Barker et al. (2021); [52] Schmidt et al. (2006); [53] Frigola et al. (2012); [54] Cortina et al. (2015); [55] Becquey & Gersonde (2003); [56] Imbrie et al. (1989); [57] Pisias & Mix (2010); [58] Hodell et al. (2000); [59] D.W. Lea (2004); [60] Irvali et al. (2019); [61] Naafs et al. 2012; [62] Clemens et al. (2018); [63] Clemens et al. (2021); [64] Bühring et al. (2004); [65] Hodell et al. (2023); [66] Lyle et al. (2002).

References

Bard, E. and Rickaby, R. E. M.: Migration of the subtropical front as a modulator of glacial climate, Nature, 460, 380–383, https://doi.org/10.1038/nature08189, 2009.

Barker, Stephen (2021): Faunal counts of planktonic foraminifera and sea surface temperatures from ODP Site 983 [dataset]. PANGAEA, https://doi.org/10.1594/PANGAEA.929742.

Barker, S., Knorr, G., Edwards, R. L., Parrenin, F., Putnam, A. E., Skinner, L. C., Wolff, E., and Ziegler, M.: 800,000 Years of Abrupt Climate Variability, Science, 334, 347–351, https://doi.org/10.1126/science.1203580, 2011.

Becquey, Sabine; Gersonde, Rainer (2003): Stable isotope analysis of benthic foraminifera and summer sea surface temperature reconstruction of sediment core PS2489-2 [dataset]. PANGAEA, https://doi.org/10.1594/PANGAEA.615929, In supplement to: Becquey, S; Gersonde, R (2003): A 0.55-Ma paleotemperature record from the Subantarctic zone: Implications for Antarctic Circumpolar Current development. Paleoceanography, 18(1), 1014, https://doi.org/10.1029/2000PA000576.

Bouchet, M., Landais, A., Grisart, A., Parrenin, F., Prié, F., Jacob, R., Fourré, E., Capron, E., Raynaud, D., Lipenkov, V. Y., Loutre, M.-F., Extier, T., Svensson, A., Legrain, E., Martinerie, P., Leuenberger, M., Jiang, W., Ritterbusch, F., Lu, Z.-T., and Yang, G.-M.: The Antarctic Ice Core Chronology 2023 (AICC2023) chronological framework

and associated timescale for the European Project for Ice Coring in Antarctica (EPICA) Dome C ice core, Clim. Past, 19, 2257–2286, https://doi.org/10.5194/cp-19-2257-2023, 2023.

Bühring, Christian; Sarnthein, Michael; Erlenkeuser, Helmut (2004): High-resolution isotope stratigraphy of ODP Site 184-1144 [dataset publication series]. PANGAEA, https://doi.org/10.1594/PANGAEA.736633.

Chen, Min-Te; Chang, Yuan-Pin; Chang, Cheng-Chieh; Wang, Liping; Wang, Chung-Ho; Yu, Ein-Fen (2002): Stable carbon and oxygen isotope ratios of Globorotalia inflata of sediment core MD96-2085 [dataset]. PANGAEA, https://doi.org/10.1594/PANGAEA.66335, In supplement to: Chen, Min-Te; Chang, Yuan-Pin; Chang, Cheng-Chieh; Wang, Li-Wen; Wang, Chung-Ho; Yu, Ein-Fen (2002): Late Quaternary sea-surface temperature variations in the southeast Atlantic: a planktic foraminifer faunal record of the past 600 000 yr (IMAGES II MD962085). Marine Geology, 180(1-4), 163-181, https://doi.org/10.1016/S0025-3227(01)00212-2.

Clemens, S. C., Prell, W. L., Sun, Y., Liu, Z., and Chen, G.: Southern Hemisphere forcing of Pliocene δ 18 O and the evolution of Indo-Asian monsoons, Paleoceanography, 23, 2008PA001638, https://doi.org/10.1029/2008PA001638, 2008.

Clemens, S. C., Holbourn, A., Kubota, Y., Lee, K. E., Liu, Z., Chen, G., Nelson, A., and Fox-Kemper, B.: Precession-band variance missing from East Asian monsoon runoff, Nat Commun, 9, 3364, https://doi.org/10.1038/s41467-018-05814-0, 2018.

Clemens, S. C., Yamamoto, M., Thirumalai, K., Giosan, L., Richey, J. N., Nilsson-Kerr, K., Rosenthal, Y., Anand, P., and McGrath, S. M.: Remote and local drivers of Pleistocene South Asian summer monsoon precipitation: A test for future predictions, Sci. Adv., 7, eabg3848, https://doi.org/10.1126/sciadv.abg3848, 2021.

Cortese, Giuseppe; Abelmann, Andrea; Gersonde, Rainer (2004): Estimation of sea surface temperatures and salinity of ODP Site 177-1089 (Appendix A) [dataset]. PANGAEA, https://doi.org/10.1594/PANGAEA.712940, Supplement to: Cortese, G et al. (2004): A glacial warm water anomaly in the subantarctic Atlantic Ocean, near the Agulhas Retroflection. Earth and Planetary Science Letters, 222(3-4), 767-778, https://doi.org/10.1016/j.epsl.2004.03.029.

Cortina Guerra, Aleix; Sierro, Francisco Javier; Flores, José-Abel; Martrat, Belén; Grimalt, Joan O (2015): Alkenone-based SST measurements from MIS 3 to MIS 11 in the northwestern Mediterranean Sea [dataset]. PANGAEA, https://doi.org/10.1594/PANGAEA.854682.

Dyez, K. A. and Ravelo, A. C.: Dynamical changes in the tropical Pacific warm pool and zonal SST gradient during the Pleistocene, Geophysical Research Letters, 41, 7626–7633, https://doi.org/10.1002/2014GL061639, 2014.

Dyez, K. A., Ravelo, A. C., and Mix, A. C.: Evaluating drivers of Pleistocene eastern tropical Pacific sea surface temperature, Paleoceanography, 31, 1054–1069, https://doi.org/10.1002/2015PA002873, 2016.
Gibson, K. A. and Peterson, L. C.: A 0.6 million year record of millennial-scale climate variability in the tropics, Geophysical Research Letters, 41, 969–975, https://doi.org/10.1002/2013GL058846, 2016.

De Garidel-Thoron, T., Rosenthal, Y., Bassinot, F., and Beaufort, L.: Stable sea surface temperatures in the western Pacific warm pool over the past 1.75 million years, Nature, 433, 294–298, https://doi.org/10.1038/nature03189, 2005.

Frigola, Jaime (2020): Borehole PRGL1-4 and sediment core MD99-2348 records from the Gulf of Lion, Mediterranean Sea: age model, Globigerina bulloides δ18O, grain-size, XRF-Ca [dataset publication series]. PANGAEA, https://doi.org/10.1594/PANGAEA.911440.

Gebhardt, Holger; Sarnthein, Michael; Grootes, Pieter Meiert; Kiefer, Thorsten; Kühn, Hartmut; Schmieder, Frank; Röhl, Ursula (2008): Stable oxygen isotopes on Neogloboquadrina pachyderma sinistral of sediment core MD01-2416 [dataset]. PANGAEA, https://doi.org/10.1594/PANGAEA.626598, In supplement to: Gebhardt, H et al. (2008): Paleonutrient and productivity records from the subarctic North Pacific for Pleistocene glacial terminations I to V. Paleoceanography, 23(4), PA4212, https://doi.org/10.1029/2007PA001513.

Gibson, K. A. and Peterson, L. C.: A 0.6 million year record of millennial-scale climate variability in the tropics, Geophysical Research Letters, 41, 969–975, https://doi.org/10.1002/2013GL058846, 2014.

Hayward, Bruce William; Scott, George H; Crundwell, Martin P; Kennett, James P; Carter, Lionel; Neil, Helen L; Sabaa, Ashwaq T; Wilson, Kate; Rodger, J Stuart; Schaefer, Grace; Grenfell, Hugh R; Li, Qianyu (2008): (Appendix 1) Census data of planktic foraminiferal faunas together with estimates of mean annual SST for ODP Site 181-1123 [dataset]. PANGAEA, https://doi.org/10.1594/PANGAEA.742593, In supplement to: Hayward, BW et al. (2008): The effect of submerged plateaux on Pleistocene gyral circulation and sea-surface temperatures

in the Southwest Pacific. Global and Planetary Change, 63(4), 309-316, https://doi.org/10.1016/j.gloplacha.2008.07.003.

Herbert, Timothy D; Lawrence, Kira T; Tzanova, Alexandrina; Peterson, Laura C; Caballero-Gill, Rocio P; Kelly, Christopher S (2018): (Table S2) SST estimates as a function of age, ODP Site 162-982 [dataset]. PANGAEA, https://doi.org/10.1594/PANGAEA.885578, In supplement to: Herbert, TD et al. (2016): Late Miocene global cooling and the rise of modern ecosystems. Nature Geoscience, 9(11), 843-847, https://doi.org/10.1038/ngeo2813.

Herbert, Timothy D; Peterson, Laura C; Lawrence, Kira T; Liu, Zhonghui (2017): Plio-Pleistocene tropical alkenone SST reconstructions for ODP Site 117-722 [dataset]. PANGAEA, https://doi.org/10.1594/PANGAEA.874749, In supplement to: Herbert, TD et al. (2010): Tropical Ocean Temperatures Over the Past 3.5 Million Years. Science, 328(5985), 1530-1534, https://doi.org/10.1126/science.1185435.

Herbert, Timothy D; Peterson, Laura C; Lawrence, Kira T; Liu, Zhonghui (2017): Plio-Pleistocene tropical alkenone SST reconstructions for ODP Site 138-846 [dataset]. PANGAEA, https://doi.org/10.1594/PANGAEA.874750, In supplement to: Herbert, TD et al. (2010): Tropical Ocean Temperatures Over the Past 3.5 Million Years. Science, 328(5985), 1530-1534, https://doi.org/10.1126/science.1185435.

Herbert, Timothy D; Peterson, Laura C; Lawrence, Kira T; Liu, Zhonghui (2017): Plio-Pleistocene tropical alkenone SST reconstructions for ODP Site 184-1146 [dataset]. PANGAEA, https://doi.org/10.1594/PANGAEA.874751, In supplement to: Herbert, TD et al. (2010): Tropical Ocean Temperatures Over the Past 3.5 Million Years. Science, 328(5985), 1530-1534, https://doi.org/10.1126/science.1185435.

Herbert, T. D., Schuffert, J. D., Andreasen, D., Heusser, L., Lyle, M., Mix, A., Ravelo, A. C., Stott, L. D., and Herguera, J. C.: Collapse of the California Current During Glacial Maxima Linked to Climate Change on Land, Science, 293, 71–76, https://doi.org/10.1126/science.1059209, 2001.

Ho, Sze Ling; Mollenhauer, Gesine; Lamy, Frank; Martínez-García, Alfredo; Mohtadi, Mahyar; Gersonde, Rainer; Hebbeln, Dierk; Nunez-Ricardo, Samuel; Rosell-Melé, Antoni; Tiedemann, Ralf (2012): Alkenone indices, sea surface temperature estimates and foraminiferal $\delta^{18}O$ of sediment core GeoB3327-5 [dataset]. PANGAEA, https://doi.org/10.1594/PANGAEA.792638, In supplement to: Ho, SL et al. (2012): Sea surface temperature variability in the Pacific sector of the Southern Ocean over the past 700 kyr. Paleoceanography, 27, PA4202, https://doi.org/10.1029/2012PA002317.

Ho, Sze Ling; Mollenhauer, Gesine; Lamy, Frank; Martínez-García, Alfredo; Mohtadi, Mahyar; Gersonde, Rainer; Hebbeln, Dierk; Nunez-Ricardo, Samuel; Rosell-Melé, Antoni; Tiedemann, Ralf (2012): Alkenone indices, sea surface temperature estimates of sediment core PS75/034-2 [dataset]. PANGAEA, https://doi.org/10.1594/PANGAEA.792639, In supplement to: Ho, SL et al. (2012): Sea surface temperature variability in the Pacific sector of the Southern Ocean over the past 700 kyr. Paleoceanography, 27, PA4202, https://doi.org/10.1029/2012PA002317.

Hodell, D. A., Charles, C. D., and Ninnemann, U. S.: Comparison of interglacial stages in the South Atlantic sector of the southern ocean for the past 450 kyr: implifications for Marine Isotope Stage (MIS) 11, 2000.

Hodell, David A; Crowhurst, Simon J; Skinner, Luke C; Tzedakis, Polychronis C; Margari, Vasiliki; Channell, James E T; Kamenov, George D; Maclachlan, Suzanne; Rothwell, Robin Guy (2013): Iberian Margin 420 kyr geochemical and color variations record [dataset publication series]. PANGAEA, https://doi.org/10.1594/PANGAEA.831762, Supplement to: Hodell, DA et al. (2013): Response of Iberian Margin sediments to orbital and suborbital forcing over the past 420 ka. Paleoceanography, 28(1), 185-199, https://doi.org/10.1002/palo.20017.

Hodell, David A; Crowhurst, Simon J; Lourens, Lucas Joost; Margari, Vasiliki; Nicolson, John; Rolfe, James E; Skinner, Luke C; Thomas, Nicola C; Tzedakis, Polychronis C; Mleneck-Vautravers, Maryline J; Wolff, Eric William (2023): Benthic and planktonic oxygen and carbon isotopes and XRF data at IODP Site U1385 and core MD01-2444 from 0 to 1.5 Ma [dataset bundled publication]. PANGAEA, https://doi.org/10.1594/PANGAEA.951401

Hodell, David A; Charles, Christopher D; Curtis, Jason H; Mortyn, P Graham; Ninnemann, Ulysses S; Venz, Kathryn A (2003): (Table T2) Stable oxygen and carbon isotope ratios of the benthic and planktonic foraminifera, carbonate content, and percent fragmentation of planktonic foraminifers for ODP Site 177-1089 in the Southern Ocean [dataset]. PANGAEA, https://doi.org/10.1594/PANGAEA.218128, In supplement to: Hodell, DA et al. (2003): Data Report: Oxygen isotope stratigraphy of ODP Leg 117 sites 1088, 1089, 1090, 1093, and 1094. In:

Gersonde, R; Hodell, DA; Blum, P (eds.) Proceedings of the Ocean Drilling Program, Scientific Results, College Station, TX (Ocean Drilling Program), 177, 1-26, https://doi.org/10.2973/odp.proc.sr.177.120.2003

Holbourn, Ann E; Kuhnt, Wolfgang; Kawamura, Hiroshi; Jian, Zhimin; Grootes, Pieter Meiert; Erlenkeuser, Helmut; Xu, Jian (2005): (Figure 2) Stable isotopes on planktic foraminifera of sediment core MD01-2378 [dataset]. PANGAEA, https://doi.org/10.1594/PANGAEA.263757, In supplement to: Holbourn, AE et al. (2005): Orbitally-paced paleoproductivity variations in the Timor Sea and Indonesian Throughflow variability during the last 460-ky. Paleoceanography, 20(3), PA3002, https://doi.org/10.1029/2004PA001094.

Howard, William R; Prell, Warren L (1992): (Table 6) Faunal dissimilarity and sea surface temperture estimates for sediment core ELT45.029 [dataset]. PANGAEA, https://doi.org/10.1594/PANGAEA.733683, In supplement to: Howard, WR; Prell, WL (1992): Late Quaternary surface circulation of the southern Indian Ocean and its relationship to orbital variations. Paleoceanography, 7(1), 79-118, https://doi.org/10.1029/91PA02994.

Howard, William R; Prell, Warren L (1992): (Table 6) Faunal dissimilarity and sea surface temperture estimates for sediment core ELT49.017-PC [dataset]. PANGAEA, https://doi.org/10.1594/PANGAEA.733684, In supplement to: Howard, WR; Prell, WL (1992): Late Quaternary surface circulation of the southern Indian Ocean and its relationship to orbital variations. Paleoceanography, 7(1), 79-118, https://doi.org/10.1029/91PA02994.

Howard, William R; Prell, Warren L (1992): (Table 6) Faunal dissimilarity and sea surface temperture estimates for sediment core ELT49.018-PC [dataset]. PANGAEA, https://doi.org/10.1594/PANGAEA.733685, In supplement to: Howard, WR; Prell, WL (1992): Late Quaternary surface circulation of the southern Indian Ocean and its relationship to orbital variations. Paleoceanography, 7(1), 79-118, https://doi.org/10.1029/91PA02994.

Howard, William R; Prell, Warren L (1992): (Table 6) Faunal dissimilarity and sea surface temperture estimates for sediment core ELT49.021-PC [dataset]. PANGAEA, https://doi.org/10.1594/PANGAEA.733686, In supplement to: Howard, WR; Prell, WL (1992): Late Quaternary surface circulation of the southern Indian Ocean and its relationship to orbital variations. Paleoceanography, 7(1), 79-118, https://doi.org/10.1029/91PA02994.

Imbrie, John D; McIntyre, Andrew (2006): SST vs time for core RC12-294 (specmap.054) [dataset]. PANGAEA, https://doi.org/10.1594/PANGAEA.441752.

Irvalı, N., Galaasen, E. V., Ninnemann, U. S., Rosenthal, Y., Born, A., and Kleiven, H. (Kikki) F.: A low climate threshold for south Greenland Ice Sheet demise during the Late Pleistocene, Proc. Natl. Acad. Sci. U.S.A., 117, 190–195, https://doi.org/10.1073/pnas.1911902116, 2020.

Jia, Q., Li, T., Xiong, Z., Steinke, S., Jiang, F., Chang, F., and Qin, B.: Hydrological variability in the western tropical Pacific over the past 700 kyr and its linkage to Northern Hemisphere climatic change, Palaeogeography, Palaeoclimatology, Palaeoecology, 493, 44–54, https://doi.org/10.1016/j.palaeo.2017.12.039, 2018.

Le, Jianning; Shackleton, Nicholas J (1992): (Table 2) Planktonic foraminifera concentrations and stable oxygen isotope ratios of sediment core ERDC-093P [dataset]. PANGAEA, https://doi.org/10.1594/PANGAEA.52476, In supplement to: Le, J; Shackleton, NJ (1992): Carbonate dissolution fluctuations in the western equatorial Pacific during the Late Quaternary. Paleoceanography, 7(1), 21-42, https://doi.org/10.1029/91PA02854.

Lea, D. W.: The 100 000-Yr Cycle in Tropical SST, Greenhouse Forcing, and Climate Sensitivity, J. Climate, 17, 2170–2179, https://doi.org/10.1175/1520-0442(2004)017<2170:TYCITS>2.0.CO;2, 2004.

Lemoine, F. (1998). Changements de l'hydrologie de surface (temperature et salinite) de l'ocean Austral en relation avec les variations de la circulation thermohaline au cours des deux derniers cycles climatiques. thesis, Univ. Paris VI, Paris.

Li, Li; Li, Qianyu; Tian, Jun; Wang, Pinxian; Wang, Hui; Liu, Zhonghui (2011): (Appendix A) Sea surface temperature reconstruction for ODP Site 184-1143 [dataset]. PANGAEA, https://doi.org/10.1594/PANGAEA.786444, Supplement to: Li, L et al. (2011): A 4-Ma record of thermal evolution in the tropical western Pacific and its implications on climate change. Earth and Planetary Science Letters, 309(1-2), 10-20, https://doi.org/10.1016/j.epsl.2011.04.016.

Li, L., Wang, H., Li, J., Zhao, M., and Wang, P.: Changes in sea surface temperature in western South China Sea over the past 450 ka, Chin. Sci. Bull., 54, 3335–3343, https://doi.org/10.1007/s11434-009-0083-9, 2009.

Lo, Li; Chang, Sheng-Pu; Wei, Kuo-Yen; Lee, Shih-Yu; Ou, Tsong-Hua; Chen, Yi-Chi; Chuang, Chih-Kai; Mii, Horng-Sheng; Burr, George S; Chen, Min-Te; Tung, Ying-Hung; Tsai, Meng-Chieh; Hodell, David A; Shen, Chuan-Chou (2019): Age model, oxygen isotopes and Mg/Ca ratios of Globigerinoides ruber from sediment core MD05-2925 off the Solomon Sea [dataset]. PANGAEA, https://doi.org/10.1594/PANGAEA.899209, In: Lo, L

et al. (2019): Age model, oxygen isotopes and Mg/Ca ratios from plantonik foraminifera of sediment core MD05-2925 off the Solomon Sea [dataset publication series]. PANGAEA, https://doi.org/10.1594/PANGAEA.899217.

Lougheed, B. C. and Obrochta, S. P.: A Rapid, Deterministic Age-Depth Modeling Routine for Geological Sequences With Inherent Depth Uncertainty, Paleoceanog and Paleoclimatol, 34, 122–133, https://doi.org/10.1029/2018PA003457, 2019.

Loulergue, L., Schilt, A., Spahni, R., Masson-Delmotte, V., Blunier, T., Lemieux, B., Barnola, J.-M., Raynaud, D., Stocker, T. F., and Chappellaz, J.: Orbital and millennial-scale features of atmospheric CH4 over the past 800,000 years, Nature, 453, 383–386, https://doi.org/10.1038/nature06950, 2008.

Lyle, M., Mix, A., & Pisias, N. (2002). Patterns of CaCO3 deposition in the eastern tropical Pacific Ocean for the last 150 kyr: Evidence for a southeast Pacific depositional spike during marine isotope stage (MIS) 2. Paleoceanography, 17(2), 3-1.

Martínez-Garcia, A., Rosell-Melé, A., Geibert, W., Gersonde, R., Masqué, P., Gaspari, V., and Barbante, C.: Links between iron supply, marine productivity, sea surface temperature, and CO 2 over the last 1.1 Ma, Paleoceanography, 24, 2008PA001657, https://doi.org/10.1029/2008PA001657, 2009.

Martínez Méndez, Gema; Zahn, Rainer; Hall, Ian R; Peeters, Frank J C; Pena, Leopoldo D; Cacho, Isabel; Negre, César (2010): Proxy records of Globigerina bulloides from splicings of MD96-2080 and MD02-2594, Agulhas Bank Splice (ABS) [dataset]. PANGAEA, https://doi.org/10.1594/PANGAEA.810663, In supplement to: Martínez Méndez, G et al. (2010): Contrasting multiproxy reconstructions of surface ocean hydrography in the Agulhas Corridor and implications for the Agulhas Leakage during the last 345,000 years. Paleoceanography, 25(4), PA4227, https://doi.org/10.1029/2009PA001879.

McManus, J. F., Oppo, D. W., and Cullen, J. L.: A 0.5-Million-Year Record of Millennial-Scale Climate Variability in the North Atlantic, Science, 283, 971–975, https://doi.org/10.1126/science.283.5404.971, 1999.

Medina-Elizalde, Martín; Lea, David W (2005): (Table S2) Stable oxygen isotope record and Mg/Ca ratios of Globigerinoides ruber from ODP Hole 130-806B [dataset]. PANGAEA, https://doi.org/10.1594/PANGAEA.772014, In supplement to: Medina-Elizalde, M; Lea, DW (2005): The Mid-Pleistocene Transition in the Tropical Pacific. Science, 310(5750), 1009-1012, https://doi.org/10.1126/science.1115933.

Naafs, Bernhard David A; Hefter, Jens; Acton, Gary D; Haug, Gerald H; Martínez-García, Alfredo; Pancost, Richard D; Stein, Ruediger (2012): Concentrations and accumulation rates of biomarkers and SSTs at IODP Site 306-U1313 [dataset]. PANGAEA, https://doi.org/10.1594/PANGAEA.757946, In supplement to: Naafs, BDA et al. (2012): Strengthening of North American dust sources during the late Pliocene (2.7 Ma). Earth and Planetary Science Letters, 317-318, 8-19, https://doi.org/10.1016/j.epsl.2011.11.026.

Nehrbass-Ahles, C., Shin, J., Schmitt, J., Bereiter, B., Joos, F., Schilt, A., Schmidely, L., Silva, L., Teste, G., Grilli, R., Chappellaz, J., Hodell, D., Fischer, H., and Stocker, T. F.: Abrupt CO 2 release to the atmosphere under glacial and early interglacial climate conditions, Science, 369, 1000–1005, https://doi.org/10.1126/science.aay8178, 2020.

Nürnberg, D., Ziegler, M., Karas, C., Tiedemann, R., and Schmidt, M. W.: Interacting Loop Current variability and Mississippi River discharge over the past 400 kyr, Earth and Planetary Science Letters, 272, 278–289, https://doi.org/10.1016/j.epsl.2008.04.051, 2008.

Nürnberg, D., Ziegler, M., Karas, C., Tiedemann, R., and Schmidt, M. W.: Interacting Loop Current variability and Mississippi River discharge over the past 400 kyr, Earth and Planetary Science Letters, 272, 278–289, https://doi.org/10.1016/j.epsl.2008.04.051, 2008.

Oppo, D. W., Linsley, B. K., Rosenthal, Y., Dannenmann, S., and Beaufort, L.: Orbital and suborbital climate variability in the Sulu Sea, western tropical Pacific, Geochem Geophys Geosyst, 4, 1–20, https://doi.org/10.1029/2001GC000260, 2003.

Pahnke, Katharina; Zahn, Rainer; Elderfield, Henry; Schulz, Michael (2003): Mg/Ca ratio and sea-surface temperature (SST) of sediment core MD97-2120 [dataset]. PANGAEA, https://doi.org/10.1594/PANGAEA.208133, In supplement to: Pahnke, K et al. (2003): 340,000-Year Centennial-Scale Marine Record of Southern Hemisphere. Science, 301(5635), 948-952, https://doi.org/10.1126/science.1084451.

Pahnke, Katharina; Zahn, Rainer; Elderfield, Henry; Schulz, Michael (2003): Stable oxygen isotopes ($\delta^{18}O$) of sediment core MD97-2120 [dataset]. PANGAEA, https://doi.org/10.1594/PANGAEA.208132, In supplement to:

Pahnke, K et al. (2003): 340,000-Year Centennial-Scale Marine Record of Southern Hemisphere. Science, 301(5635), 948-952, https://doi.org/10.1126/science.1084451.

Paillard, D., Labeyrie, L., and Yiou, P.: Macintosh Program performs time-series analysis, EoS Transactions, 77, 379–379, https://doi.org/10.1029/96EO00259, 1996.

Peeters, F. J. C., Acheson, R., Brummer, G.-J. A., De Ruijter, W. P. M., Schneider, R. R., Ganssen, G. M., Ufkes, E., and Kroon, D.: Vigorous exchange between the Indian and Atlantic oceans at the end of the past five glacial periods, Nature, 430, 661–665, https://doi.org/10.1038/nature02785, 2004.

Peterson, L. C., Lawrence, K. T., Herbert, T. D., Caballero-Gill, R., Wilson, J., Huska, K., Miller, H., Kelly, C., Seidenstein, J., Hovey, D., and Holte, L.: Plio-Pleistocene Hemispheric (A)Symmetries in the Northern and Southern Hemisphere Midlatitudes, Paleoceanog and Paleoclimatol, 35, e2019PA003720, https://doi.org/10.1029/2019PA003720, 2020.

Pisias, N. G. and Mix, A. C.: Spatial and temporal oceanographic variability of the eastern equatorial Pacific during the Late Pleistocene: Evidence from radiolaria microfossils, Paleoceanography, 12, 381–393, https://doi.org/10.1029/97PA00583, 1997.

Rodrigues, Teresa; Voelker, Antje H L; Grimalt, Joan O; Abrantes, Fatima F; Naughton, Filipa (2011): Sea surface temperature reconstruction for the middle Pleistocene from sediment core MD03-2699 [dataset]. PANGAEA, https://doi.org/10.1594/PANGAEA.761771, Supplement to: Rodrigues, T et al. (2011): Iberian Margin Sea Surface Temperature during MIS 15 to 9 (580-300 ka): Glacial suborbital variability versus interglacial stability. Paleoceanography, 26, PA1204, https://doi.org/10.1029/2010PA001927.

Romero, Oscar E; Kim, Ji-Hoon; Bárcena, María Angeles; Hall, Ian R; Zahn, Rainer; Schneider, Ralph R (2018): Alkenone concentration and sea surface temperature of sediment core MD02-2588 [dataset]. PANGAEA, https://doi.org/10.1594/PANGAEA.895560, In supplement to: Romero, OE et al. (2015): High-latitude forcing of diatom productivity in the southern Agulhas Plateau during the past 350 kyr. Paleoceanography, 30(2), 118-132, https://doi.org/10.1002/2014PA002636.

Ronge, Thomas A; Tiedemann, Ralf (2014): Mg/Ca ratio and calculated sea surface temperature of sediment core MD06-2986 [dataset]. Alfred Wegener Institute, Helmholtz Centre for Polar and Marine Research, Bremerhaven, PANGAEA, https://doi.org/10.1594/PANGAEA.835641.

Rosell-Melé, Antoni; Martínez-García, Alfredo; McClymont, Erin L (2014): Alkenone accumulation rates and SST reconstruction for ODP Site 175-1084 [dataset]. PANGAEA, https://doi.org/10.1594/PANGAEA.841832, In supplement to: Rosell-Melé, A et al. (2014): Persistent warmth across the Benguela upwelling system during the Pliocene epoch. Earth and Planetary Science Letters, 386, 10-20, https://doi.org/10.1016/j.epsl.2013.10.041

Ruddiman, William F; Raymo, Maureen E; Martinson, Douglas G; Clement, Bradford M; Backman, Jan (1989): (Table A2) Sea surface temperature reconstruction of DSDP Site 94-607 in the North Atlantic [dataset]. PANGAEA, https://doi.org/10.1594/PANGAEA.52373, In supplement to: Ruddiman, WF et al. (1989): Pleistocene evolution: northern hemisphere ice sheets and North Atlantic Ocean. Paleoceanography, 4(4), 353-412, https://doi.org/10.1029/PA004i004p00353.

Sarnthein, Michael (1997): Stable isotope analysis on planktic and benthic foraminifera on sediment core profile GeoB1113-4/-7 [dataset]. PANGAEA, https://doi.org/10.1594/PANGAEA.54395.

Schmidt, M. W., Vautravers, M. J., and Spero, H. J.: Western Caribbean sea surface temperatures during the late Quaternary, Geochem Geophys Geosyst, 7, 2005GC000957, https://doi.org/10.1029/2005GC000957, 2006.

Scussolini, Paolo; Peeters, Frank J C (2013): The record of stable isotope composition of surface and thermocline planktic foraminifera from sediment core 64PE-174P13 for the last 460,000 years [dataset]. PANGAEA, https://doi.org/10.1594/PANGAEA.825688, Supplement to: Scussolini, P; Peeters, FJC (2013): A record of the last 460 thousand years of upper ocean stratification from the central Walvis Ridge, South Atlantic. Paleoceanography, 28(3), 426-439, https://doi.org/10.1002/palo.20041.

Shackleton, N. J., Berger, A., and Peltier, W. R.: An alternative astronomical calibration of the lower Pleistocene timescale based on ODP Site 677, Transactions of the Royal Society of Edinburgh: Earth Sciences, 81, 251–261, https://doi.org/10.1017/S0263593300020782, 1990.

Stuut, Jan-Berend W; Prins, Maarten Arnoud; Schneider, Ralph R; Weltje, Gert Jan; Jansen, J H Fred; Postma, George (2002): (Fig. 2) Stable oxygen istopes on planktic foraminifera of sediment core MD96-2094 [dataset]. PANGAEA, https://doi.org/10.1594/PANGAEA.230294, In supplement to: Stuut, J-BW et al. (2002): A 300-kyr

record of aridity and wind strength in southwestern Africa: inferences from grain-size distributions of sediments on Walvis Ridge, SE Atlantic. Marine Geology, 180(1-4), 221-233, https://doi.org/10.1016/S0025-3227(01)00215-8.

Tachikawa, K., Timmermann, A., Vidal, L., Sonzogni, C., and Timm, O. E.: CO2 radiative forcing and Intertropical Convergence Zone influences on western Pacific warm pool climate over the past 400ka, Quaternary Science Reviews, 86, 24–34, https://doi.org/10.1016/j.quascirev.2013.12.018, 2014.

Venz, Kathryn A; Hodell, David A; Stanton, Cathy; Warnke, Detlef A (1999): Stable carbon and oxygen isotope ratios of planktonic and benthic foraminifera from ODP Site 162-982 in the North Atlantic [dataset]. PANGAEA, https://doi.org/10.1594/PANGAEA.700897, Supplement to: Venz, KA et al. (1999): A 1.0 myr record of glacial North Atlantic Intermediate Water variability from ODP Site 982 in the northeast Atlantic. Paleoceanography, 14(1), 42-52, https://doi.org/10.1029/1998PA900013.

Voelker, Antje H L; Rodrigues, Teresa; Billups, Katharina; Oppo, Delia W; McManus, Jerry F; Stein, Ruediger; Hefter, Jens; Grimalt, Joan O (2010): Stable carbon and oxygen isotopic compsoition of Globorotalia inflata of sediment core MD03-2699 [dataset]. PANGAEA, https://doi.org/10.1594/PANGAEA.742785, In supplement to: Voelker, AHL et al. (2010): Variations in mid-latitude North Atlantic surface water properties during the mid-Brunhes (MIS 9-14) and their implications for the thermohaline circulation. Climate of the Past, 6(4), 531-552, https://doi.org/10.5194/cp-6-531-2010.

Voelker, Antje H L; de Abreu, Lucia (2011): Stable oxygen and carbon isotope ratios of Globigerina bulloides of sediment core MD95-2040 [dataset]. PANGAEA, https://doi.org/10.1594/PANGAEA.737413, In supplement to: Voelker, AHL; de Abreu, L (2011): A Review of Abrupt Climate Change Events in the Northeastern Atlantic Ocean (Iberian Margin): Latitudinal, Longitudinal and Vertical Gradients. In: Rashid, H; Polyak, L; Mosley-Thompson, E (eds.), Abrupt Climate Change: Mechanisms, Patterns, and Impacts. Geophysical Monograph Series (AGU, Washington D.C.), 193, 15-37, https://doi.org/10.1029/2010GM001021.

Windler, G., Tierney, J. E., DiNezio, P. N., Gibson, K., and Thunell, R.: Shelf exposure influence on Indo-Pacific Warm Pool climate for the last 450,000 years, Earth and Planetary Science Letters, 516, 66–76, https://doi.org/10.1016/j.epsl.2019.03.038, 2019.

Zhang, Shuai; Yu, Zhoufei; Gong, Xun; Wang, Yue; Chang, Fengming; Li, Tiegang (2021): Sable oxygen isotope and Mg/Ca ratios of planktonic foraminifera from KX97322-4 (KX22-4) [dataset]. PANGAEA, https://doi.org/10.1594/PANGAEA.939377.

Ziegler, M., Lourens, L. J., Tuenter, E., and Reichart, G.-J.: High Arabian Sea productivity conditions during MIS 13 – odd monsoon event or intensified overturning circulation at the end of the Mid-Pleistocene transition?, Clim. Past, 6, 63–76, https://doi.org/10.5194/cp-6-63-2010, 2010.